GEOPHYSICS, VOL. 51, NO. 9 (SEPTEMBER 1986); P. 1830-1849, 9 FIGS., 2 TABLES.

Theory of induced-polarization logging in a borehole

R. Freedman* and J. P. Vogiatzis‡

ABSTRACT

Currently, there is interest by the petroleum well-logging industry in the potential use of induced polarization (IP) measurements to improve formation evaluation in shaly sands. Shell Development Company has constructed an experimental four-electrode IP and resistivity logging tool to obtain downhole measurements in shaly sands. This study contributes to the theoretical understanding and interpretation of the dynamic (i.e., time-dependent) response of this type of downhole IP logging device.

A low-frequency (e.g., 32 Hz or less) electric current oscillating at a single fixed frequency is applied between a pair of current electrodes in a borehole. The resulting voltages induced between pairs of potential measuring electrodes in the borehole are calculated by solving the time-dependent Maxwell's equations. Inductive electromagnetic (EM) coupling contributions to apparent (e.g., measured) IP phase angles are automatically taken into account. The model is applied to the study of normal logging arrays for which the voltage measuring electrodes are interior to the current electrodes. The model responses are calculated for normal arrays in both infinitely thick noninvaded formations and infinitely thick invaded formations. EM coupling contributions to apparent IP phase angles have an approximately universal dependence on a scaling parameter defined here. The scaling relationship permits the quantitative estimate of EM coupling effects for specific tool parameters (i.e., electrode spacings and frequencies) and formation characteristics (i.e., apparent conductivities). Therefore, scaling relationships of this type should be useful in the design of IP tools. An inverse method, developed for determining true formation IP phase angles and resistivities from apparent values measured by an IP tool, utilizes data from multiple pairs of voltage-measuring electrodes and exploits the fact that, for the systems of interest, the inverse resistivity and IP problems can be "decoupled."

The assumption that IP phase angles have a logarithmic dependence on frequency over a decade frequency interval leads to a nonlinear relationship between percent frequency effect (PFE) and IP phase angle. This nonlinear relationship agrees well with experimental data.

INTRODUCTION

Background

Induced polarization (IP) phenomena were discovered more than fifty years ago (Allaud et al., 1977, 30–34; Schlumberger, 1920). The discovery and documentation are credited to C. Schlumberger who discovered the IP effect while conducting surface exploration measurements in the search for metallic ore deposits. Schlumberger's field measurements involved establishing electric currents in the earth and measuring potential differences between pairs of reference electrodes. He observed that when the electric currents were interrupted, the measured potential differences decayed very slowly. The decay rate was much slower than could be accounted for by the finite conductivity of the earth. The earth appeared to be acting like a giant capacitor that had been polarized by the applied current and was then discharging. One of the many intriguing aspects of IP is that wet rocks containing metallic minerals and/or clays can exhibit effective relative dielectric constants, at frequencies below 1.0 Hz, as large as 10^8 (Fuller and Ward, 1970). These large dielectric constants are more than six orders of magnitude greater than the dielectric constants of the rock constituents (e.g., brine, hydrocarbons, clays, metallic minerals, etc.).

The physics of the IP phenomena cannot be understood simply in terms of the bulk properties of the rock constituents. Most physical models (Sumner, 1976) which attempt to explain IP focus on the interactions between cations in the brine and electric charges (electrons in the case of metallic minerals and anions in the case of clay minerals) at the mineral surfaces. A different approach has recently been discussed by Sen

Manuscript received by the Editor February 28, 1985; revised manuscript received February 13, 1986.
*Schlumberger Well Services, P.O. Box 2175, Houston, TX 77252-2175.
‡Shell Development Co., P.O. Box 481, Houston, TX 77001.

LIST OF SYMBOLS

$\mathbf{A}$ = Vector potential defined via equation (12) (A).

a = Borehole radius (m).

AM, AN = Distances separating the A electrode from the M and N electrodes, respectively.

$\mathbf{B} = \mu_0 \mathbf{H}$ = Magnetic induction (W/m^2).

BM, BN = Distances separating the B electrode from the M and N electrodes, respectively.

$\mathbf{D} = \varepsilon' \mathbf{E}$ = Electric displacement vector ($coulomb/m^2$).

$\mathbf{E}$ = Electric field intensity (V/m).

$F^{(i)}(R_1, R_2, b)$ = Deviations of theoretically computed apparent resistivities from their measured values as defined in equation (28) ($\Omega \cdot m$).

$FE \equiv PFE/100$ = Frequency effect (dimensionless).

$\mathbf{H}$ = Magnetic field intensity (A-turn/m).

I = Amplitude (i.e., peak value) of the alternating current $I_T(t)$.

$I_T(t)$ = Alternating current in the insulated cables connecting the A and B electrodes to the power supply (A).

$\mathbf{J}_s$ = Current density in the insulated cable separating the A and B electrodes defined in equation (20) (A/m^2).

K = True effective relative dielectric constant of a medium (dimensionless).

k = Complex propagation constant defined in equation (19) (m^{-1}).

L_e^2 = Effective length squared as defined in equation (27).

PFE = Percent frequency effect defined in equation (C-2). (dimensionless).

R_a = Apparent formation resistivity defined in equation (4) ($\Omega \cdot m$).

$R_a^{(i)}$ = Measured values of apparent resistivity where superscripts $i = 1, 2, 3$ denote a particular set of electrode spacings ($\Omega \cdot m$).

$\bar{R}_a^{(i)}(R_1, R_2, b)$ = Theoretically computed values of apparent resistivities where R_1, R_2, and b denote the invaded zone resistivity, the uninvaded zone resistivity and the invaded zone radius, respectively ($\Omega \cdot m$).

R_m = Resistivity of drilling mud ($\Omega \cdot m$).

R_t = Formation resistivity ($\Omega \cdot m$).

R_{x0} = Invaded zone resistivity ($\Omega \cdot m$).

r_{x0} = Invaded zone radius (m).

t = Time (s).

$V(\rho_0, z)$ = complex phasor voltage from which $V_{MN,I}$ and $V_{MN,Q}$ are calculated using equations (22) and (23), respectively (V).

V_0 = Amplitude of $V_{MN}(t)$ (V).

$V_{MN}(t)$ = Complex voltage induced between the measuring electrodes M and N (V).

$V_{MN,Q}$ = Quadrature voltage component induced between the measuring electrodes M and N (V).

$V_{MN,I}$ = In-phase voltage component induced between the measuring electrodes M and N (V).

$z_M \equiv AM$ = See definition of AM (m).

$z_N \equiv AN$ = See definition of AN (m).

$\delta = (2/\omega\mu_0\sigma)^{1/2}$ = Classical EM skin depth where $\mu_0 = 4\pi \times 10^{-7}$ H/m is the magnetic permeability of a vacuum (m).

$\varepsilon' = K\varepsilon_0$ = Dielectric constant of a medium (F/m).

$\varepsilon_0 = (36\pi)^{-1} \times 10^{-9}$ = Dielectric constant of a vacuum (F/m).

θ = IP parameter of a medium as defined in equation (6) (radians).

θ_t = Formation IP parameter (radians).

θ_{x0} = Invaded zone IP parameter (radians).

$\bar{\theta}_a^{(i)}$ = Measured values of apparent formation phase angles from which EM effects have been subtracted (mradians).

θ_a = Apparent formation phase angles defined in equation (5) (mradians).

$\Delta\theta$ = EM coupling contribution to apparent phase angles as defined in equation (25).

μ = Magnetic permeability of a medium (H/m).

ρ_0 = Radial coordinate of the measuring electrode cables (m).
ρ_t = True charge density (see Maxwell's equations).
(ρ, ϕ, z) = Cylindrical coordinates.
σ = Conductivity of a medium (S/m).
σ^* = Complex conductivity defined in equation (17) (S/m).
Φ = Scalar potential defined in equation (14) (V).
ω = Angular frequency of the alternating current provided by the power supply. Also the frequency of the resulting electromagnetic fields (radians/s).

Subscripts

a denotes apparent formation parameter.
t denotes formation parameter.
$x0$ denotes invaded zone parameter.
m denotes borehole or drilling mud parameter.

(1981). He considers a model which focuses on the role of geometrical effects and argues that the large dielectric constants in rocks can be caused by the presence of rock grains with high aspect ratios. In spite of the voluminous literature on the IP effect, the complexity of the problem has led to considerable controversy and there are no generally accepted models which explain all of the IP observed phenomena.

The primary commercial application of IP has been for exploration of metallic ore deposits by surface IP measurements. The effects of EM coupling and the theory of IP surface measurements have been studied extensively in connection with mineral exploration (Dey and Morrison, 1973; Wynn and Zonge, 1977; Nair and Sanyal, 1980; Madden and Cantwell, 1967). The ability of IP to detect disseminated sulfide minerals has also been used to estimate the sulphur content, and, therefore, the quality of in-situ coal deposits. By comparison, the use of IP to evaluate or locate petroleum reservoirs has not been commercially successful. The early work on applying IP to the in-situ study of petroleum reservoirs was conducted in the U.S.S.R. Dakhnov et al. (1952) describe IP well-logging field equipment and discuss both laboratory and field IP measurements. Their interpretation of the field measurements is qualitative, but their field data suggest that IP might be useful for identification of lithology and for locating permeable zones. IP and spontaneous potential (SP) logs in shaly sands have the same general character.

During the decade 1950–1960, the development and use of IP for mineral exploration grew, while interest in IP for petroleum reservoir studies seemed to decline. In the past decade, a number of publications have revived interest in applying IP borehole logging to evaluation of shaly sand reservoirs. Hoyer and Rumble (1976) give experimental data which indicate that the dielectric constants of shaly sands are approximately linearly proportional to their cation exchange capacities (Q_v). The paper by Snyder et al. (1977) reviews the state-of-the-art in IP well-logging methods and expresses the belief that borehole measurements might permit the in-situ measurement of Q_v in shaly sand reservoirs. More extensive studies of IP in shaly sands have recently been reported by Vinegar and Waxman (1984). Their results confirm the results of Hoyer and Rumble (1976) and lead to a model equation for the quadrature conductivity of shaly sands. Vinegar et al. (1985) report on tool development, borehole departure curves, and field tests of an experimental downhole IP tool constructed at Shell Development Company for IP logging of shaly sands.

Previous work and scope of this paper

In spite of decades of research on IP, there has been little work in the literature on quantitative modeling of the borehole responses of IP tools. Brant and The Newmont Exploration Staff (1966) calculate borehole departure curves for a model zero-frequency IP device consisting of two point electrodes in a borehole. This pioneering effort failed to address a number of important aspects of downhole IP logging, including the inverse problem for the effects of invasion and the effects of EM coupling on the tool response. Vinegar et al. (1985) present borehole IP and resistivity departure curves computed using Seigel's (1959) coupling-free theory of IP. Vinegar et al. treated EM coupling using an approximation based on expressions derived by Sunde (1948) and Wait (1959) valid in an infinite homogeneous medium. The paper by Vinegar et al. (1985) did not address the inverse invasion problem for IP logging.

A dynamic model for studying the responses of downhole unfocused four-electrode electrical logging devices is discussed. The model and the theory underlying it provide a consistent analysis of resistivity and IP logging in a borehole. The model permits obtaining apparent formation resistivities and IP parameters from measured logging data. The exact dynamic response of the model is calculated, and EM contributions to apparent resistivities and apparent IP parameters are taken into account automatically. True formation resistivities and IP parameters are obtained from the apparent values by solving appropriate boundary value and inverse problems. Examples illustrate under what conditions true formation resistivities and IP parameters can be obtained from measured tool responses. The results discussed here are valid for (1) an infinitely thick, noninvaded formation penetrated by a borehole, and (2) an infinitely thick invaded formation penetrated by a borehole. The model's use in other logging geometries is not considered.

In addition to the inductive coupling effects from wave propagation, there are also capacitive coupling effects from current leakage between the current and potential-measuring wires and electrodes (Wait, 1959; Madden and Cantwell,

1967). We consider an idealized model and neglect the capacitive coupling which can also obscure the true IP response of the formation. In practice these effects can be minimized by prudent tool design (Vinegar et al., 1985).

Previous works on IP have frequently assumed a linear relationship between the two most widely used IP parameters, percent frequency effect (PFE) and phase angle (Zonge et al., 1972). We derive a nonlinear relationship between them. In the limit of small phase angles (e.g., shaly sands), this relationship is approximately linear and is in excellent agreement with the experimental data of Vinegar and Waxman (1984). In rocks containing metallic minerals, the phase angles can be large and the nonlinear relationship proposed here also compares favorably with the experimental data of Zonge et al. (1972).

Downhole instrumentation and measurements

Figure 1 displays a schematic of a model four-electrode IP logging device. In practice the power supply, phase-sensitive detector, and amplifier are located downhole (Vinegar and Waxman, 1982). The electrode system which consists of point electrodes A, B, M, and N is suspended from an armored cable (not shown). During the logging operation, the electrode system is raised and lowered in the borehole at fixed distances between the electrodes. For the logging method described here, the borehole must contain a conductive drilling mud, that is, wells drilled with oil-base muds cannot be logged. A power supply provides an alternating current $I_T(t)$ of fixed angular frequency ω and amplitude I in the insulated cable between the current electrodes A and B. This results (via Maxwell's equations) in an oscillating voltage $V_{MN}(t)$ being induced between the M and N electrodes which are connected by insulated cables to a phase-sensitive detector and amplifier. The induced voltage $V_{MN}(t)$ also oscillates at angular frequency ω (i.e., because of the linearity of Maxwell's equations), but in general the voltage will be out-of-phase with $I_T(t)$. The mathematical relationship is as follows. If the current has the form

$$I_T = I \cos \omega t, \tag{1}$$

then the induced voltage will be of the form

$$V_{MN}(t) = V_0 \cos (\omega t - \theta_a), \tag{2}$$

where V_0 is the amplitude of the oscillating voltage and θ_a is an apparent phase angle which describes the phase relation between $I_T(t)$ and $V_{MN}(t)$. Note that the induced voltage in equation (2) consists of a component $V_{MN,I}$ which oscillates in-phase with I_T and a quadrature component $V_{MN,Q}$ which oscillates 90 degrees out-of-phase with I_T. Equation (2) shows that

$$V_{MN,I} \equiv V_0 \cos \theta_a, \tag{3a}$$

and

$$V_{MN,Q} \equiv V_0 \sin \theta_a. \tag{3b}$$

A phase-sensitive detector such as the one shown in Figure 1 measures both the in-phase and quadrature components of the induced voltage. The in-phase voltage component is utilized to determine an apparent formation resistivity. The quadrature component of the induced voltage which contains the IP response is not measured in conventional resistivity logging. An experimental four-electrode IP tool which operates according to principles similar to those described has been constructed by Shell Development Company (Vinegar et al., 1985).

Definition of apparent formation resistivities and phase angles

The in-phase and quadrature voltage components measured by an apparatus such as that in Figure 1 can be used to define apparent resistivities R_a and apparent phase angles θ_a. The apparent resistivity (in $\Omega \cdot$ m) is obtained from $V_{MN,I}$ using the

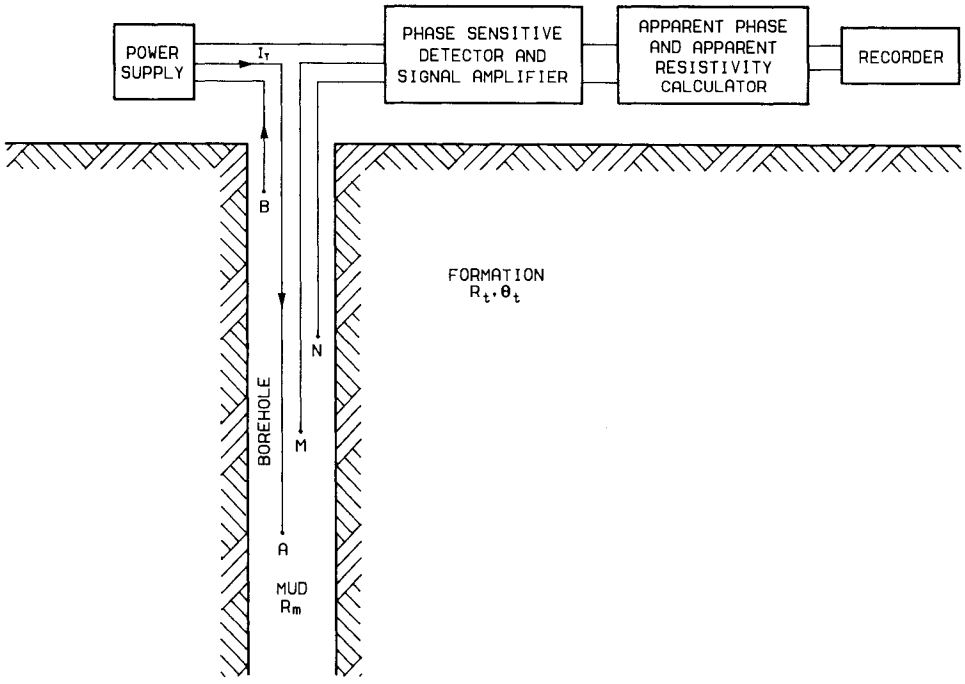

FIG. 1. A schematic of a four-electrode normal IP logging tool.

relation

$$R_a = \frac{4\pi}{I} V_{MN,I}\left(\frac{1}{AM} - \frac{1}{AN} + \frac{1}{BN} - \frac{1}{BM}\right)^{-1}, \quad (4)$$

where AM, AN, BN, and BM are the distances (in meters) separating the electrodes. The above definition of R_a is similar to the definition in the conventional theory of unfocused point electrode-type resistivity devices (Dakhnov, 1959). In the latter case, the in-phase voltage component in equation (4) is replaced by the voltage amplitude (V_0). This difference is negligible for IP logging in shaly sands since, for the expected range of measured phase angles (i.e., less than 100 mradians), V_0 and $V_{MN,I}$ differ by less than 1 percent. The apparent phase angles θ_a in milliradians are defined by

$$\theta_a = 1\,000 \tan^{-1} \frac{V_{MN,Q}}{V_{MN,I}}. \quad (5)$$

A major aim of this paper is to demonstrate under what conditions the true formation resistivities R_t and IP parameters θ_t can be determined from R_a and θ_a. We define the IP parameter θ (in radians) by

$$\theta = \tan^{-1} \frac{\omega\varepsilon_0 K}{\sigma}, \quad (6)$$

where K is an effective relative dielectric constant for the medium, $\varepsilon_0 = (36\pi)^{-1} \times 10^{-9}$ F/m is the dielectric permittivity of a vacuum, and σ is the effective conductivity of the medium in units of S/m (Fuller and Ward, 1970). Note that σ is simply the reciprocal of the resistivity $R(\Omega \cdot m)$. Therefore, if R_t and θ_t can be determined from the downhole tool response, then the effective formation relative dielectric constant K_t can be determined from equation (6). Thus IP logging in shaly sands can be viewed as a method for dielectric constant logging at low frequencies (e.g., 32 Hz or less).

The argument of the arctangent in equation (6) is the ratio of the quadrature and real parts of the complex conductivity of the medium. IP parameters defined by equation (6) are identical to the IP phase angles which Vinegar and Waxman (1984) measured in their laboratory experiments on shaly sand core samples. The ratio of the quadrature and real parts of the complex conductivity in shaly sands is typically less than 0.03. Therefore, an excellent approximation for the IP parameter of a shaly sand is

$$\theta \simeq \frac{\omega\varepsilon_0 K}{\sigma}. \quad (6a)$$

DYNAMIC MODEL OF ELECTRODE-TYPE ELECTRICAL LOGGING TOOLS

Time-dependent Maxwell's equations, potentials and gauge conditions

The starting point of our treatment of the dynamic response of electrode-type electrical logging tools is Maxwell's equations in the frequency domain, which in mks units are

$$\nabla \times \mathbf{E} = i\omega\mathbf{B}, \quad (7)$$

$$\nabla \times \mathbf{H} = -i\omega\mathbf{D} + \sigma\mathbf{E} + \mathbf{J}_s, \quad (8)$$

$$\nabla \cdot \mathbf{B} = 0, \quad (9)$$

$$\nabla \cdot \mathbf{D} = \rho_t \quad (10)$$

with

$$\mathbf{B} = \mu\mathbf{H},$$

and (11)

$$\mathbf{D} = \varepsilon'\mathbf{E},$$

where $\varepsilon' = K\varepsilon_0$ is the effective dielectric constant and μ is the magnetic permeability of the medium.

Note that the dielectric constant, and therefore the IP effect, enters Maxwell's equations through the displacement current term in equation (8). The magnetic permeability μ can be replaced by the permeability of a vacuum, $\mu_0 = 4\pi \times 10^{-7}$ H/m. This is an excellent approximation for nonferromagnetic media since the deviations of μ from μ_0 arising from paramagnetic effects are negligible. The current density $\mathbf{J}_s$ is a source current arising from the alternating current in the cable separating the A and B electrodes.

To solve Maxwell's equations (7)–(10), it is convenient to cast them in terms of a vector potential $\mathbf{A}$ and a scalar potential Φ. First, we introduce $\mathbf{A}$ by observing that since $\nabla \cdot \mathbf{H} = 0$,

$$\mathbf{H} = \nabla \times \mathbf{A}. \quad (12)$$

To introduce ϕ, substitute the equation (12) into equation (7) and use the constitutive relation $\mathbf{B} = \mu_0 \mathbf{H}$. Thus

$$\nabla \times [\mathbf{E} - i\omega\mu_0 \mathbf{A}] = 0, \quad (13)$$

and therefore the quantity in brackets can be written as the negative gradient of a scalar potential. Thus, we arrive at a familiar result

$$\mathbf{E}(\omega) = -\nabla\Phi + i\omega\mu_0 \mathbf{A}. \quad (14)$$

Note that in obtaining equation (14), we have taken time Fourier transforms using the convention that any function of time $S(t)$ is related to its transform $\tilde{S}(\omega)$ via

$$S(t) = \int_{-\infty}^{\infty} \frac{d\omega}{2\pi} \tilde{S}(\omega) e^{i\omega t}. \quad (15)$$

On substituting equations (12) and (14) into equation (8) and using the constitutive relations in equation (11), after some straightforward algebra, a coupled equation for $\mathbf{A}$ and ϕ is obtained. This equation can be decoupled by choosing the gauge condition

$$\Phi = -\frac{\nabla \cdot \mathbf{A}}{\sigma^*}, \quad (16)$$

which provides a relationship between the potentials. In equation (16), we have introduced the complex conductivity

$$\sigma^* = \sigma(1 - i\theta), \quad (17)$$

where $\theta = \omega\varepsilon'/\sigma$ is an IP parameter. On using the gauge condition the vector potential obeys the inhomogeneous wave equation

$$\nabla^2\mathbf{A} + k^2\mathbf{A} = -\mathbf{J}_s(\mathbf{r}), \quad (18)$$

where the complex propagation constant

$$k = \frac{(1+i)}{\delta}(1 - i\theta)^{1/2}, \quad (19)$$

has been introduced and where $\delta = (2/\omega\mu_0\sigma)^{1/2}$ is the classical skin depth.

Equations (18) and (19) are general; in order to specify our model, it is necessary to choose an appropriate source current

density $\mathbf{J}_s(\mathbf{r})$. For an electrode-type electrical logging tool such as the one depicted in Figure 1, we choose $\mathbf{J}_s(\mathbf{r})$ to be of the form [in a cylindrical coordinate system (ρ, ϕ, z) with origin at the A electrode],

$$\mathbf{J}_s(\mathbf{r}) = -\frac{I\delta(\rho)[u(z) - u(z-L)]\mathbf{e}_z}{2\pi\rho}, \tag{20}$$

where $u(z)$ is a unit step function defined by the equation

$$u(z) = \begin{cases} 1, & \text{for } z \geq 0 \\ 0, & \text{for } z < 0 \end{cases}. \tag{21}$$

$\mathbf{e}_z$ is a unit vector in the z direction, and $L = \mathrm{AB}$ is the distance separating the A and B electrodes. Also, note that the current density vanishes everywhere except along the portion of the insulated current cable which is between the A and B electrodes. Moran and Gianzero (1979) discuss a similar model in an investigation of the interplay of resistivity anisotropy and finite frequency effects on the apparent resistivities of electrical logging tools.

Definition of the forward problem and a method for calculating apparent formation resistivities and IP parameters

The model described permits calculation of the voltage components $V_{\mathrm{MN},I}$ and $V_{\mathrm{MN},Q}$ (and therefore θ_a and R_a) for an electrode-type logging tool operating at any frequency and for any prescribed electrode-spacing and configuration. The EM coupling effects contribute to θ_a and can mask the small IP response of the formation if they are not taken into account properly. The EM coupling effects decrease with decreasing frequency and also with decreasing electrode spacings AM and AN. Therefore, it is possible to decrease the EM effects by decreasing the electrode spacings; however, this decreases the depth of investigation.

The values of θ_a and R_a determined from the solution of our model depend not only on tool parameters (e.g., frequency, electrode spacings, etc.), but also on borehole and formation properties. For example, consider an infinitely thick bed penetrated by a borehole and having an invaded zone of radius r_{x0}. The tool response, and hence θ_a and R_a, in this zone depends upon (1) the borehole radius (a), (2) the drilling-mud resistivity (R_m), (3) the invaded-zone radius (r_{x0}), (4) the invaded-zone resistivity (R_{x0}), (5) the invaded-zone IP parameter (θ_{x0}), (6) the formation resistivity (R_t), and (7) the formation IP parameter (θ_t). In a more complex model for the formation the tool response will, of course, depend upon more parameters. Given any model for the formation and values for all of the parameters which define the model, then, in principle, the values of θ_a and R_a can be computed. We call this a solution of the "forward problem" for the model.

The solution of the forward problem for a given model of the formation involves solving the Maxwell's equations (just discussed). These equations lead to mathematical boundary-value problems which can be solved analytically for all of the standard logging geometries normally considered in modeling logging tool responses. For more complex geometries (e.g., invaded thin beds), our dynamic model equations can be solved numerically using finite-element and/or finite-difference methods. We do not consider these more complicated situations here. In Appendix A, we use Green's function and integral transform methods to obtain analytical solutions to our model equations for the following logging geometries: (1) an infinitely thick, uninvaded bed penetrated by a borehole; and (2) an infinitely thick, invaded bed penetrated by a borehole.

The detailed results of our calculations are too lengthy to display here; however, it is useful to discuss them in general. Our calculations result in a complex voltage $V(\rho, z)$ (i.e., a phasor voltage in electrical engineering terminology) from which the in-phase ($V_{\mathrm{MN},I}$) and quadrature ($V_{\mathrm{MN},Q}$) voltage components induced between the M and N electrodes can be computed. These voltage components are obtained from the equations

$$V_{\mathrm{MN},I} = \mathrm{Re}\,[V(\rho_0, z_M) - V(\rho_0, z_N)], \tag{22}$$

and

$$V_{\mathrm{MN},Q} = \mathrm{Im}\,[V(\rho_0, z_M) - V(\rho_0, z_N)], \tag{23}$$

where Re and Im are operators which take the real and imaginary parts, respectively, of the complex quantities on which they operate; ρ and z denote coordinates in a cylindrical coordinate system [i.e., (ρ, ϕ, z)] whose origin is at the A electrode. The coordinate ρ_0 is the radial coordinate of the voltage measuring cables; $z_M = \mathrm{AM}$ and $z_N = \mathrm{AN}$ are electrode spacings. The bracketed terms in equations (22) and (23) are line integrals of the electric field along a path connecting the M and N electrodes, e.g.,

$$V(\rho_0, z_M) - V(\rho_0, z_N) \equiv \int_{z_M}^{z_N} d\mathbf{s} \cdot \mathbf{E}(\rho_0, z). \tag{24}$$

In Appendix A the boundary-value problem for our dynamic model is solved for the two logging geometries considered. An expression for $V(\rho_0, z)$ is derived [see equation (A-26)] which, together with equations (A-22) and (A-40), represent our solutions. These equations, together with equations (A-25a) and A-25b), were used to calculate θ_a and R_a for the examples presented here. In Appendix B, our dynamic model is solved in an infinite homogeneous medium. The inductive EM coupling terms obtained in Appendix B are shown to agree with those obtained previously by Wait (1959) in computing the transfer impedance between parallel wires in an infinite, homogeneous medium.

EM coupling contributions to apparent IP phase angles

The numerical results below illustrate the EM coupling contributions to apparent IP phase angles for four-electrode normal IP arrays.

The EM coupling contributions ($\Delta\theta$) to the apparent IP phase angles for an IP tool operating at a frequency f are defined by

$$\Delta\theta = \theta_a(f) - \theta_a(f_0), \tag{25}$$

where θ_a are apparent IP phase angles defined in equation (5) and f_0 is a low frequency (i.e., essentially dc) for which EM coupling contributions are negligible. The numerical results presented below were obtained using $f_0 = 2^{-6}(0.015\,6)$ Hz.

We consider four-electrode normal arrays for which the B electrode is located in the borehole. Calculations of $\Delta\theta$ were performed for several different IP arrays in a borehole penetrating an infinitely thick noninvaded formation. For these situations, the tool responses were computed using equations (A-25), (A-26), (4), and (5).

Our numerical results demonstrate the following.

(1) $\Delta\theta$ has a negligible dependence on the formation IP parameter (θ_t) for the systems of interest for which $0 \leq \theta_t \leq 30$ mradians and $f \leq 32$ Hz.

(2) The dominant contribution to $\Delta\theta$ is from the term in equation (A-26) which contains the modified Bessel function K_0.

Some insight into the scaling behavior of $\Delta\theta$ can be obtained by extracting the dominant contribution to $\Delta\theta$ from the K_0 term in equation (A-26). After some straightforward algebra, we find that

$$\Delta\theta \approx 2\pi L_e^2 f \sigma_a \mu_0 \ln\left(\frac{\sqrt{2\pi\mu_0 f\sigma_m}}{2}\rho_0\right) + \cdots, \quad (26)$$

where we have introduced an "effective length" squared for a four-electrode normal array which is defined by

$$L_e^2 = (\mathrm{AN} - \mathrm{AM})\left(\frac{1}{\mathrm{AM}} - \frac{1}{\mathrm{AN}} + \frac{1}{\mathrm{BN}} - \frac{1}{\mathrm{BM}}\right)^{-1}. \quad (27)$$

Note that if the B electrode were at infinity (e.g., in the mud pit), then $L_e^2 = (\mathrm{AM})(\mathrm{AN})$, as might be expected. In deriving equation (26), we have used a well-known small-argument expansion for the modified Bessel function, i.e., $K_0(z^*) = (-1/2)\ln(z^*/2) + \cdots$, valid for $z^* \to 0$.

In equation (26), σ_a and σ_m are the apparent formation and drilling mud conductivities, respectively, and $\Delta\theta$ is in radians. All of the calculations were done using $\rho_0 = 0.01$ m for the radial coordinate of the voltage-measuring electrodes. $\Delta\theta$ is negative [the negative sign comes from the logarithm in equation (26)] for the normal arrays considered here.

The form of $\Delta\theta$ in equation (26) suggests that the EM coupling contributions to apparent IP phase angles can be scaled using the scaling parameter $L_e^2 \sigma_a f$. Numerical calculations of $\Delta\theta$ were performed as a function of $L_e^2 \sigma_a f$ for (1) 8-inch and 12-inch borehole diameters, (2) resistivity ratios (R_t/R_m) in the range from 1 to 60, and (3) for the three sets of electrode spacings shown in Figure 2. We find the dependence of $\Delta\theta$ on the scaling parameter is approximately universal. That is, for fixed values of $L_e^2 \sigma_a f$, we found only slight differences in $\Delta\theta$ for different values of f, R_t/R_m, electrode spacings, and borehole size. Figure 2 displays approximate upper and lower bounds on $\Delta\theta$ obtained from the calculations. The closeness of the bounds illustrates the approximately universal nature of the scaling. The weak, nonuniversal dependences on R_t/R_m and electrode spacings result from the other terms (i.e., the terms not involving the modified Bessel function K_0) in equation (A-26). These terms do not scale like $L_e^2 \sigma_a f$, because they have a different z dependence (i.e., dependence on electrode spacing) than the dominant K_0 term. Figures 3 through 5 display resistivity departure curves which were also generated by the calculations described above. The latter results showed that the apparent formation resistivities (R_a) have negligible dependences on f and θ_t. Figure 2 can be used to estimate the

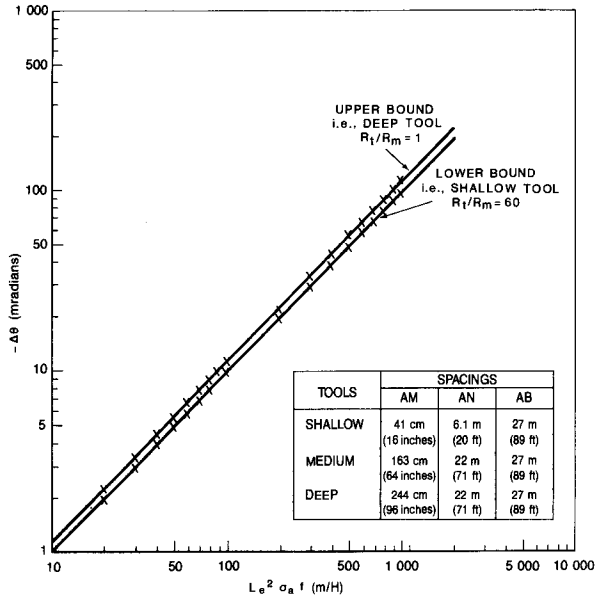

FIG. 2. Approximate upper and lower bounds for EM coupling contributions to apparent IP phase angles.

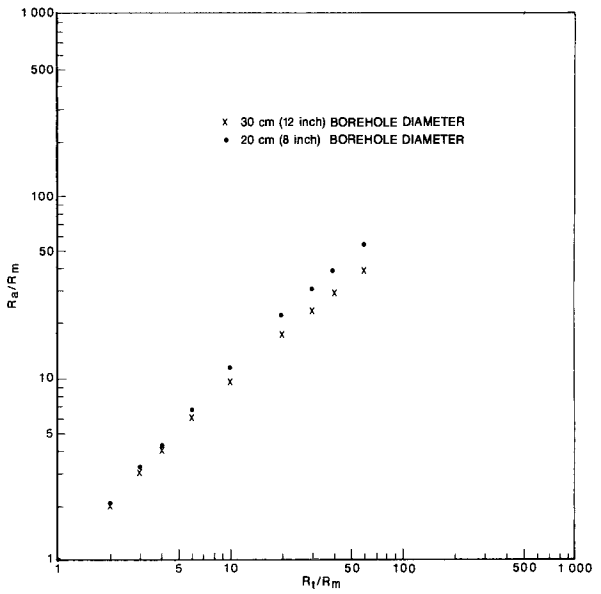

FIG. 3. Resistivity departure curves for shallow tool.

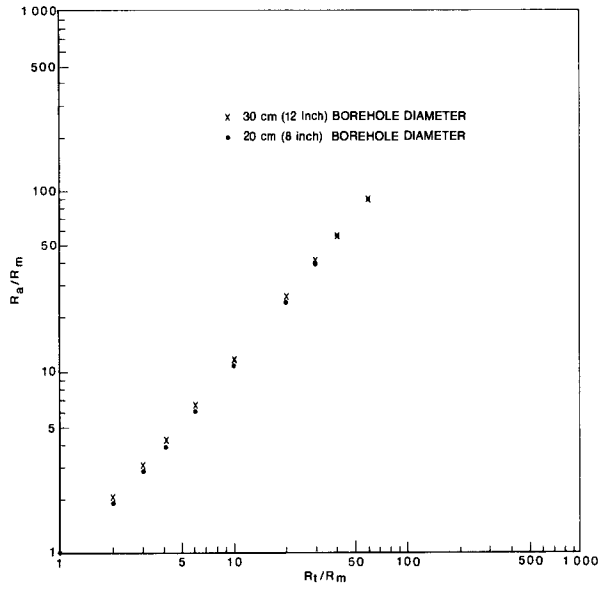

FIG. 4. Resistivity departure curves for medium tool.

magnitude of the EM coupling contributions to $\Delta\theta$ for different tool designs. For example, if $-\Delta\theta$ must be less than approximately 10 mrad, then $L_e^2 \sigma_a f \lesssim 100$. This latter inequality places obvious constraints on the tool frequencies and electrode spacings for any anticipated range of apparent resistivities.

Note that if $L_e^2 \sigma_m f$ had been used as the scaling parameter, then Figure 2 would have consisted of a family of curves for $\Delta\theta$ corresponding to different values of R_t/R_m. Use of σ_a instead of σ_m in the definition of the scaling parameter results in the almost total coalescence of this family of curves (Figure 2).

Note also that the findings reported here are valid only for four-electrode normal arrays with the B electrode in the borehole. The EM coupling effects for other arrays can be similarly investigated and will generally have different characteristics (e.g., see Nair and Sanyal, 1980).

Definition of the inverse problem and a method for obtaining IP parameters, resistivities, and invasion radii from logging data

To define and illustrate the "inverse problem" we consider the simple model for invasion discussed earlier. That is, we consider a borehole of known radius $\rho = a$ is filled with a drilling mud having known resistivity R_m and IP parameter $\theta_m = 0$. The annular region $a \le \rho \le r_{x0}$ is invaded by the borehole fluid and has electrical properties R_{x0} and θ_{x0}. The region $\rho > r_{x0}$ is the uninvaded formation and has electrical parameters R_t and θ_t. The response of an IP tool in this borehole will, therefore, depend functionally on five unknown parameters (i.e., θ_{x0}, R_{x0}, θ_t, R_t, and r_{x0}). Thus at least five independent measurements are required to determine these parameters. Determining these parameters from the logging data (i.e., measured voltages) involves the solution of an inverse problem. This inverse problem can be described as follows: Suppose that one is given five independent measurements of the response of an IP tool. Furthermore, suppose we have a method for calculating these responses for any set of values of the five unknown parameters (this is the forward problem). It is then possible to devise a method (discussed below) for determining values of the unknown parameters such that the calculated responses are identical to the input (i.e., measured) responses. If the set of parameters determined is unique, then we have solved the inverse problem. In Figure 6, we display a schematic of an IP device having three sets of electrode spacings (a set consists of electrode pairs AB, AM, and AN). This device can measure three apparent resistivities and three apparent IP parameters and can, therefore, provide enough data to find a solution of the inverse problem.

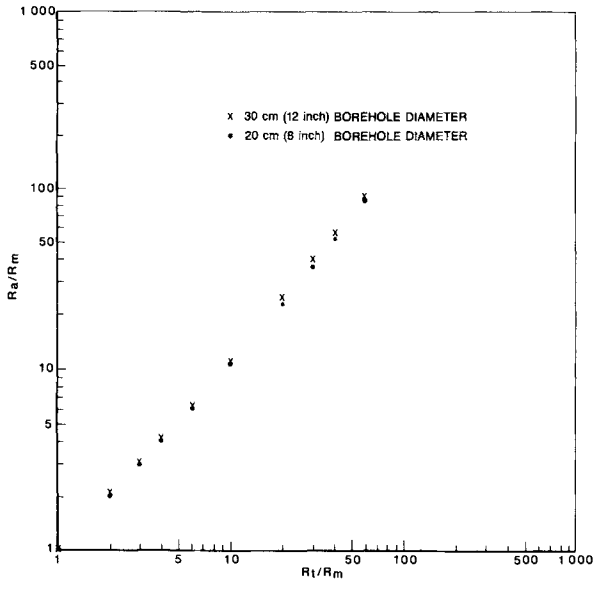

FIG. 5. Resistivity departure curves for deep tool.

We briefly describe our method for solving the inverse problem discussed above. An example of this method for a particular case is presented and discussed next. Let $R_a^{(i)}$ denote measured values of apparent resistivity where subscripts $i = 1, 2, 3$ refer to the particular set of electrode spacings for which $R_a^{(i)}$ is determined. Let $\bar{R}_a^{(i)}(R_1, R_2, b)$ denote the theoretically computed values (i.e., solutions of the forward problem) of apparent resistivities. We are using the fact that the theoretically computed apparent resistivities have a negligible dependence on EM and IP effects for the devices and application considered here. This leads to a "decoupling" of the resistivity and IP inverse problems. That is, the inverse resistivity problem can be solved and the solution can then be used to solve the inverse IP problem. The theoretically computed values for fixed i depend functionally on the values assigned to (1) the resistivity of the invaded zone (R_1), (2) the resistivity of the formation zone (R_2), and (3) the radius of the invaded zone (b). In a more complex model, the computed values of apparent resistivity will depend upon more parameters. Generalization of this inverse method to more complex models is straightforward, however, an IP tool with more than three sets of electrode spacings is required to obtain values of formation IP parameters and resistivities.

It is convenient to introduce the deviations of the computed values of the apparent resistivities from their corresponding measured values. That is, we define the functions

$$F^{(i)}(R_1, R_2, b) \equiv \bar{R}_a^{(i)}(R_1, R_2, b) - R_a^{(i)}, \tag{28}$$

for $i = 1, 2, 3$. The solution of the inverse problem for the present model involves determining values of the parameters R_1, R_2, and b such that the deviations $F^{(i)}(R_1, R_2, b)$ vanish. The values thus determined are the values predicted by the model for R_{x0}, R_t, and r_{x0}. The method we use to obtain the zeroes of equation (28) is a simple iterative scheme based on the well-known Newton-Raphson method for solving systems of nonlinear equations (Kunz, 1957). Application of this method to equations (28) leads to a set of algebraic recursion relations (for $i = 1, 2, 3$),

$$\Delta R_1^{n+1} \frac{\partial F^{(i)}}{\partial R_1} + \Delta R_2^{n+1} \frac{\partial F^{(i)}}{\partial R_2} + \Delta b^{n+1} \frac{\partial F^{(i)}}{\partial b} + F^{(i)} = 0, \tag{29}$$

where $\Delta R_1^{n+1} = R_1^{n+1} - R_1^n$, etc., and $n = 0, 1, 2, \ldots$ is an iteration index. A procedure for obtaining initial values $R_1^{(0)}$, $R_2^{(0)}$, and $b^{(0)}$ for the iteration scheme is discussed in the next section. The functions $F^{(i)}$ and their partial derivatives in the above equations are evaluated at R_1^n, R_2^n, and b^n. Convergence of the iteration occurs after M iterations provided that the absolute values of the ratios $\Delta R_1^M/R_1^M$, $\Delta R_2^M/R_2^M$, and $\Delta b^M/b^M$ are all less than a prescribed error criterion. On convergence of the scheme one automatically obtains the desired model parameters, i.e., $R_{x0} = R_1^M$, $R_t = R_2^M$, and $r_{x0} = b^M$. Note that

at each step of the iteration process in equation (29) it is necessary to compute $F^{(i)}$ and its derivatives. Therefore, to solve the inverse problem one must have accurate and rapid methods for solving the forward problem.

The next step in solving the inverse problem is determination of the IP parameters θ_{x0} and θ_t. Using a relationship derived by Balabanian and Bickart (1969), the set of approximate equations

$$\bar{\theta}_a^{(i)} = \frac{\theta_{x0} R_{x0}}{R_a^{(i)}} \frac{\partial F^{(i)}}{\partial R_1} + \frac{\theta_t R_t}{R_a^{(i)}} \frac{\partial F^{(i)}}{\partial R_2} \tag{30}$$

can be derived. In equation (30), the $\bar{\theta}_a^{(i)}$ are measured values of apparent formation phase angles from which the EM coupling contributions ($\Delta\theta$) have been subtracted. The EM coupling contributions to be subtracted from the measured apparent phase angles are defined in equation (26) and are computed as previously described. A derivation of equation (30) is given in Appendix D, and the method is applied to the inverse resistivity and IP problem for an infinitely thick, invaded formation. The derivatives in equation (30) are evaluated at $R_1 = R_{x0}$, $R_2 = R_t$, and $b = r_{x0}$. Note that these same derivatives are computed in the final iteration of equation (29) so that the only unknowns in equation (30) are θ_{x0} and θ_t. Thus, apparent phase angles $\bar{\theta}_a^{(i)}$ (i.e., with EM coupling contributions subtracted) from only two sets of electrode spacings are required to determine θ_{x0} and θ_t. In the next section we discuss an application of our inverse method. In the example discussed, the formation is deeply invaded (i.e., the invaded-zone radius is equal to six borehole radii) and the invaded-zone parameters (θ_{x0}, R_{x0}) and formation parameters (θ_t, R_t) are significantly different. This example represents a situation where the effects of invasion on the tool response are severe, so it is a good test of the validity of the method.

PREDICTIONS AND RESULTS FROM THEORETICAL MODELS

Departure curves for an infinitely thick noninvaded bed penetrated by a borehole

Figure 7 displays a graphical relationship between θ_a and R_a and the formation parameters θ_t and R_t. These curves were obtained by using equations (A-22) and (A-26) to calculate values of θ_a and R_a for different values of θ_t and R_t. These curves represent a graphical solution of the inverse problem for an infinitely thick, noninvaded bed penetrated by a borehole since, with them, θ_t and R_t can be obtained from values of θ_a and R_a. The departure curves depicted are valid for an IP tool in an 8 inch borehole filled with a relatively high-resistivity mud having $R_m = 1\ \Omega \cdot m$. Note that $\theta_m = 0$ since most drilling fluids do not exhibit IP effects. The departure curves in Figure 7 demonstrate that significant borehole effects must be correctly accounted for to determine R_t and θ_t from the apparent values θ_a and R_a determined from the tool response. For example, if the tool records values $R_a = 80\ \Omega \cdot m$ and $\theta_a = 20$ mradians, then from the departure curves $R_t = 100\ \Omega \cdot m$ and $\theta_t = 30$ mradians. The departure curves also illustrate the effects of frequency on the response of an IP tool. At two frequencies considered in Figure 7, 1 Hz and 10 Hz, for the electrode spacings and borehole conditions considered, the frequency effects are most important for the lower values of formation resistivity. Observe also that for small values of θ_t the apparent values θ_a can be negative at higher frequencies. The departure curves in Figure 7 are valid for an IP tool whose electrode spacings and configurations are identical to the standard 16-inch (41 cm) normal tool used in resistivity logging. Similar departure curves can easily be constructed for any set of electrode spacings and for any borehole size and mud resistivity.

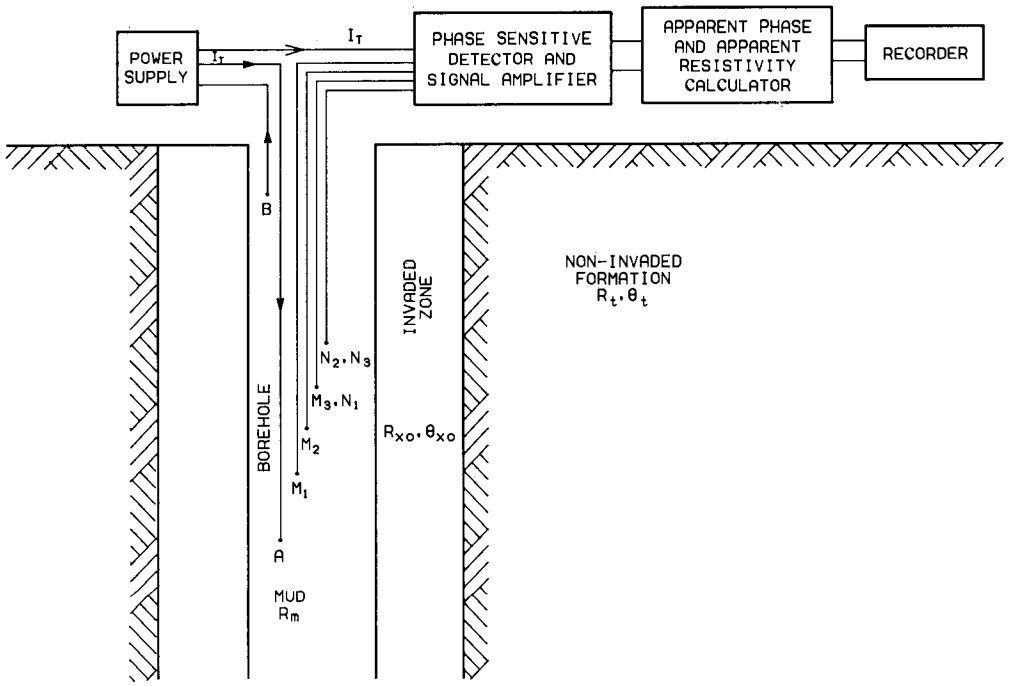

FIG. 6. A schematic of IP device with three sets of electrode spacings.

Pseudodeparture curves for an infinitely thick invaded bed penetrated by a borehole

The usefulness of departure curves of the type discussed above is lessened when the formation is invaded by mud filtrate, because of the proliferation of unknown parameters which occurs whenever the formation is invaded. To illustrate this point, consider a simple model for the invasion. A borehole of known radius $\rho = a$ is assumed to be filled with a drilling mud with known resistivity R_m and IP parameter $\theta_m = 0$. The annular region $a \leq \rho \leq r_{x0}$ is invaded by the borehole fluid and has electrical parameters R_{x0} and θ_{x0}. The tool response in this borehole will, therefore, depend upon five unknown parameters (i.e., θ_{x0}, R_{x0}, θ_t, R_t, and r_{x0}). There are clearly too many variables to display graphically. Nevertheless constructing "pseudodeparture curves" lends some light on the invasion problem. That is, suppose the properties of the invaded zone (i.e., values of R_{x0}, θ_{x0}, and r_{x0}) are given. For fixed values of the invaded-zone properties we can construct, using equations (A-26), (A-40), and (A-41), pseudodeparture curves such as those in Figures 8 and 9. Figure 8 shows coupling-free (i.e., zero-frequency) pseudodeparture curves illustrating the effects of invasion on the response of an IP device having electrode spacings identical to the standard 64-inch normal tool. Note that EM coupling effects (dashed curve) can be quite large at these relatively long electrode spacings. Figure 9 depicts a pseudodeparture curve for the same situation shown in Figure 8, except that the electrode spacings are those of the 16-inch (41 cm) normal tool. A comparison of Figures 8 and 9 shows that the response of the longer-spaced tool is much more sensitive to the formation properties (i.e., θ_t and R_t). Indeed, if the radius of the invaded zone in Figure 9 is increased from two to six borehole radii, then the 16-inch normal response becomes essentially insensitive to the properties of the formation. The sensitivity of the longer-spaced tool (i.e., 64-inch normal) is reduced when the

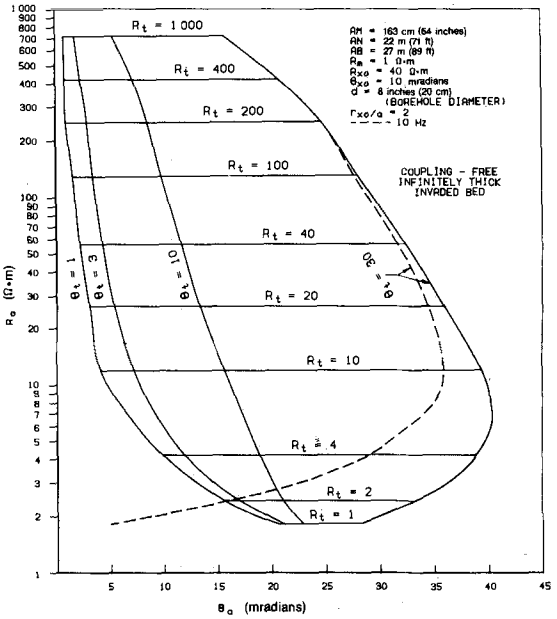

FIG. 8. A pseudodeparture curve for the effects of invasion on the response of an IP device with electrode spacings identical to those of a 64-inch (163 cm) normal tool.

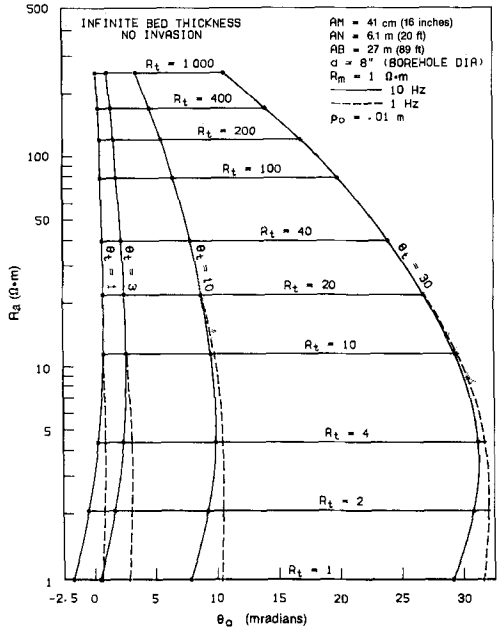

FIG. 7. A borehole departure curve for an IP device whose electrode spacings and configuration are identical to those of a 16-inch (41 cm) normal tool.

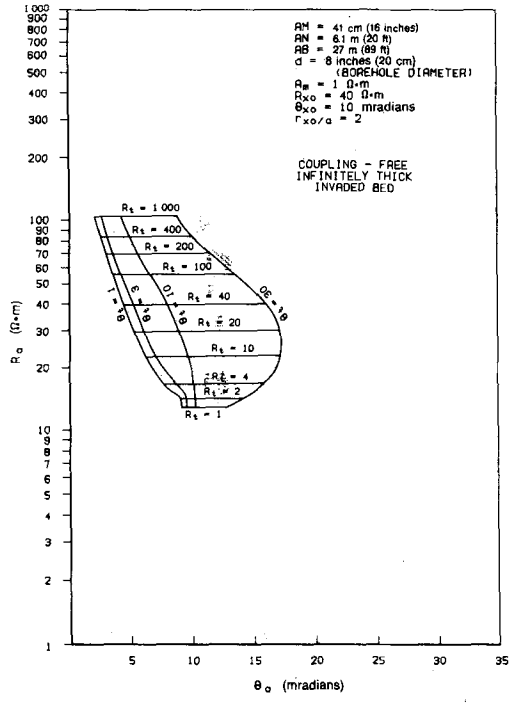

FIG. 9. A pseudodeparture curve for the effects of invasion on the response of an IP device with electrode spacings identical to those of a 16-inch (41 cm) normal tool.

Table 1. Application of the inverse method to a deeply invaded formation.

a = 0.102 m (BOREHOLE RADIUS)

R_m = Ω·m (MUD RESISTIVITY)

ELECTRODE SPACINGS (m) AND APPARENT VALUES

AM	AN	AB*	$R_a^{(i)}$	$\bar{\theta}_a^{(i)}$
0.406	6.10	∞	12.75	3.67
1.62	21.64	∞	122.77	6.80
6.10	21.64	∞	415.46	8.34

STEP 1: DETERMINATION OF R_{xo}, R_t AND r_{xo}

n	$R_1^{(n)}$	$R_2^{(n)}$	$b^{(n)}$
-	12.747	415.461	0.305
1	9.288	414.957	0.341
2	6.921	426.257	0.379
3	5.342	450.149	0.418
4	4.250	486.582	0.456
5	3.557	541.478	0.493
6	3.020	602.848	0.523
7	2.693	669.789	0.548
8	2.374	736.378	0.598
9	2.193	796.629	0.581
10	2.072	846.303	0.590
11	1.993	883.928	0.596
12	1.972	918.875	0.601
13	1.968	945.351	0.604
14	1.971	964.378	0.606
15	1.977	977.450	0.607
16	1.983	986.103	0.608
17	1.988	991.644	0.609
18	1.992	995.091	0.609
19	1.995	997.180	0.609
21	1.998	999.129	0.610
22	1.999	999.532	0.610
23	1.999	999.754	0.610
24	2.000	999.873	0.610
25	2.000	999.937	0.610

*B-ELECTRODE IN THE MUD PIT.

STEP 2: DETERMINATION OF θ_{xo} AND θ_t

ELECTRODE SPACINGS	θ_{xo}	θ_t
$\bar{\theta}_a^{(1)}$, $\bar{\theta}_a^{(2)}$	10.06	31.11
$\bar{\theta}_a^{(1)}$, $\bar{\theta}_a^{(3)}$	10.06	31.09
$\bar{\theta}_a^{(2)}$, $\bar{\theta}_a^{(3)}$	10.33	31.11

radius of the invaded zone is increased to six borehole radii; however, there is still good sensitivity to the formation properties. This suggests that at least two of the sets of electrode spacings on the device in Figure 6 should be chosen to provide a greater depth of investigation than the 16-inch normal spacing.

Application of the inverse method to a deeply invaded formation

This example demonstrates the accuracy and efficiency of the inverse procedure for obtaining values of R_{x0}, θ_{x0}, R_t, θ_t, and r_{x0} from the apparent resistivities and IP parameters obtained from a tool such as the one in Figure 6. Consider a tool with three sets of electrode spacings identical to those of standard 16-inch (41 cm), 64-inch (163 cm) and 20-ft (6.1 m) normal devices. Moreover, consider this tool situated in a borehole of radius $a = 0.102$ m which penetrates an infinitely thick invaded bed with invaded zone radius $r_{x0} = 0.610$ m. In this example we consider invaded-zone properties $R_{x0} = 2$ Ω·m, $\theta_{x0} = 10$ mradians, and formation properties $R_t = 1\,000$ Ω·m and $\theta_t = 30$ mradians. The deep invasion (i.e., six-borehole radii) and the large contrast in invaded-zone and formation properties make this example a formidable test case for our inverse method. The apparent values of resistivity $R_a^{(i)}$ and $\bar{\theta}_a^{(i)}$ obtained by measurements with the three sets of electrode spacings are listed in Table 1. Note that $i = 1, 2, 3$ denotes, respectively, the 16-inch (41 cm), 64-inch (163 cm), and 20-ft (6.1 m) normal spacings. Table 1 shows that the apparent values of resistivities and IP parameters are very different from the actual or true values. To determine true values from the apparent values, we use the two-step procedure discussed in the preceding section. First, we solve the set of iterative equations (28). Initial values for the iteration procedure are obtained as follows. The initial value of the invaded zone resistivity is set equal to the apparent resistivity from the 16-inch (41 cm) normal, i.e., $R_1^{(0)} = R_a^{(1)}$, and the initial value of the formation resistivity is set equal to the apparent resistivity from the 20-ft (6.1 m) normal, i.e., $R_2^{(0)} = R_a^{(3)}$. The initial value of the invaded-zone radius is set equal to three borehole radii, i.e., $b^{(0)} = 3a$. Table 1 lists the values of $R_1^{(n)}$, $R_2^{(n)}$, and $b^{(n)}$ obtained at each step of the iteration. Note that after 25 iterations we have obtained values of R_{x0}, R_t, and r_{x0} accurate to within one-tenth of 1 percent.

This computation required 4.5 minutes on a UNIVAC 1108. Note that each step of the iteration required four solutions of the forward problem. Thus, in this example we solved the forward problem 100 times, supporting our assertion that accurate and rapid solutions of the forward problem are essential to solution of the inverse problem. The next step is to utilize the values obtained for R_{x0}, R_t, and r_{x0} to obtain true IP parameters θ_{x0} and θ_t from the measured apparent values $\bar{\theta}_a^{(i)}$ (from which EM coupling contributions have been subtracted). This is simple and merely involves solution of any pair of the set of three algebraic equations (30). Table 1 displays results obtained by using all three pairs of equations to determine θ_{x0} and θ_t. In practice any inconsistencies between solutions arrived at by using different pairs would be warnings that either the model is inadequate (e.g., thin beds or other effects might be important) or that the logging data are poor. Note that the values of θ_{x0} and θ_t obtained using different pairs of spacings are in good agreement.

Comparison of a nonlinear relationship between percent frequency effect and IP phase angle with laboratory data

In Appendix C a nonlinear relationship between percent frequency effect (PFE) and IP phase angle is derived. The PFE is simply the percent change in resistivity per decade change in frequency. The PFE and phase angle are the two most commonly used parameters to characterize IP phenomena. Previous workers on the IP effect have frequently utilized linear relationships between the IP phase angle and PFE.

Appendix C demonstrates that a linear relationship is valid only in the regime of small phase angles, or more precisely, when $2\theta/\pi \ln 10 \ll 1$, where θ is in radians and is evaluated at the geometric mean $(\sqrt{\omega_1\omega_2})$ of the two frequencies of interest. This inequality is satisfied for shaly sandstones where true formation IP phase angles are not expected to exceed approximately 30 mradians (Vinegar and Waxman, 1984). In the mining industry where the IP effect is widely used to identify rock strata containing metallic minerals, this inequality is violated. In this case phase angles of hundreds of milliradians are frequently of interest. The nonlinear relationship derived in Appendix C is

$$\mathrm{PFE} = 100\left[\exp\left(\frac{2\theta}{\pi}\ln\frac{\omega_2}{\omega_1}\right) - 1\right]. \qquad (31)$$

In the limit of small phase angles we can expand the exponential in the above equation and obtain

$$\mathrm{PFE} \cong 0.146\ 6\theta \qquad (\theta \text{ in milliradians}). \qquad (32)$$

As noted in Appendix C, the constant of proportionality (0.1466) is in excellent agreement with the experimental results of Vinegar and Waxman (1984) on 20 shaly sandstone samples saturated with brine. Table 2 compares the predictions of the nonlinear (NL) relationship with experimental data obtained by Zonge et al. (1972). They measured both the frequency effect FE (PFE/100) and the phase angle on a suite of mineralized rocks composed of a variety of mineral types and concentrations of conductive materials. The frequency measurements were performed at 0.1 and 1.0 Hz. Table 2 lists the measured FE and phase angle θ in columns 2 and 3, respectively. In column 4 we have computed, using the measured phase angles, the FE predicted using a theoretical relationship (FE = 1.8θ) derived by Zonge et al. This relationship is discussed in Appendix C. The fifth column of Table 2 lists the FE predicted by equation (31) using the measured phase angles. It is clear that the NL relationship derived in Appendix C is in better agreement with Zonge et al.'s data than is the linear relationship they derived. Indeed only for sample MOR-4 does the FE predicted by the Zonge et al. relationship agree better with the measured FE than does the NL relationship.

SUMMARY AND CONCLUSIONS

A dynamic (i.e., time-dependent) model of unfocused electrode-type electrical logging devices has been proposed to study resistivity and IP logging in a borehole. The model has been applied to study the frequency-domain responses of four-electrode normal type devices in shaly sand formations. The dynamic model self-consistently accounts for inductive EM coupling effects on apparent IP phase angles (θ_a). The EM coupling effects on θ_a have been studied in detail for four-electrode normal arrays and are shown to have an approximately universal dependence on a scaling parameter $L_e^2\sigma_a f$.

Determination of true formation resistivities and IP parameters from apparent values requires solution of an inverse

Table 2. Comparison of the nonlinear (NL) relationship with laboratory data and theory of Zonge et al. (1972).

SAMPLE*	FE(0.1, 1.0)	$\theta^{\ddagger}$(0.316 Hz)	FE = 1.8 θ	FE (NL)
TB-15-1	0.002 3	0.001 9	0.003 4	0.002 8
Y-4125-A	0.018	0.012	0.022	0.018
MOR-1	0.054	0.035	0.063	0.053
MINN-1	0.057	0.036	0.065	0.054
TB-24-40	0.077	0.048	0.086	0.073
MOR-2	0.097	0.061	0.110	0.094
MOR-4	0.190	0.110	0.200	0.170
MOR-3	0.360	0.210	0.380	0.360
AN-810A	0.410	0.240	0.40	0.420
MIN-2	0.680	0.350	0.630	0.670

*SAMPLES ARE DESCRIBED IN TABLE 1 OF ZONGE et al. (1972).

$^{\ddagger}\theta$ IS IN RADIANS.

problem. A new two-step method which permits accurate and rapid solution of the inverse problem for the dynamic model has been proposed. As an example of the method, we demonstrated how values of R_{x0}, R_t, θ_{x0}, θ_t, and r_{x0} can be determined from logging data acquired in a deeply invaded formation.

The two most widely used IP parameters are phase angle (θ) and percent frequency effect (PFE). We demonstrated that a linear relationship between these two parameters is, in general, not valid. We derived a nonlinear relationship which is in good agreement with published experimental data over the whole range of physical interest.

Note added in proof.—After this work was completed, H. J. Vinegar brought to our attention the work of Van Voorhis et al. (1973). They presented a different derivation of the nonlinear relationship developed here.

ACKNOWLEDGMENTS

We thank Shell Development Company for permission to publish this paper. We thank J. D. Robinson for his interest in this work and for helpful conversations during the course of this work. Also we thank E. Baskir, E. G. Flowers, D. R. Montague and J. Olivé for their help in the preparation and review.

REFERENCES

Abramowitz, M., and Stegun, I. A. Eds., 1964, Handbook of mathematical functions: National Bureau of Standards, applied mathematics series, **55**, 375.

Allaud, L. A., and Martin, M. H., 1977, Schlumberger: The history of a technique: John Wiley and Sons.

Balabanian, N., and Bickart, T. A., 1969, Electrical network theory: John Wiley and Sons, Inc., 433–447.

Brant, A. A., and The Newmont Exploration Staff, 1966, Examples of induced polarization field results in the time domain: Mining Geophysics, **1**, Soc. Explor. Geophys.

Dakhnov, V. N., 1959, The application of geophysical methods; electrical well logging: Moscow Petroleum Institute; trans., G. V. Keller (1962), Colorado School of Mines Quart., **57**.

Dakhnov, V. N., Latishova, M. G., and Ryapolov, V. A., 1952, Investigation of wells by the induced polarization method (electrolytic well logging): Sb. Promislovaya Geofizika, Vnetoneft; trans., G. V. Keller: The Log Analyst, November-December, 46–82.

Dey, A., and Morrison, F., 1973, Electromagnetic coupling in frequency and time-domain induced-polarization surveys over a multilayered earth: Geophysics, **38**, 380–405.

Erdelyi, A., 1954, Bateman manuscript project, tables of integral transforms, Vol. II.: McGraw-Hill Book Co., 17.

Fuller, B. D., and Ward, S. H., 1970, Linear system description of the electrical parameters of rocks: Inst. Electr. and Electron. Eng., Trans. Geosci. Electron., **GE-8**, 7–18.

Hoyer, W. A., and Rumble, R. C., 1976, Dielectric constant of rocks as a petrophysical parameter: Soc. Prof. Well Log Analysts 17th Ann. Logging Symp., Denver, paper 0.

Kunz, K. S., 1957, Numerical analysis: McGraw-Hill Book Co.

Madden, T. R., and Cantwell, T., 1967, Induced polarization, a review: Mining Geophysics, **1**, Theory, Soc. Explor. Geophys., 373–400.

Moran, J. H., and Gianzero, S., 1979, Effects of formation anisotropy on resistivity-logging measurements: Geophysics, **44**, 1266–1286.

Nair, M. R., and Sanyal, N., 1980, Electromagnetic coupling in IP measurements using some common electrode arrays over a uniform half-space: Geoexplor., **18**, 97–109.

Runge, R. J., Worthington, A. E., and Lucas, D. R., 1969, Ultra-long spaced electric log (ULSEL): Trans., Soc. Prof. Well-log Analysts H-1-22.

Schlumberger, C., 1920, Étude sur la Prospection Électrique du Sous-Sol: Gauthier-Villars et Cie.

Sen, P. N., 1981, Relation of certain geometrical features to the dielectric anomaly of rocks: Geophysics, **46**, 1714–1720.

Seigel, H. O., 1959, A theory of induced polarization effects (for step-function excitation), *in* Wait, J. R., Ed., Overvoltage research and geophysical applications: Pergamon Press, 4–21.

Sunde, E. D., 1948, Earth conduction effects in transmission systems: D. Van Nostrand Co., 30–31.

Snyder, D. D., Merkel, R. H., and Williams, J. T., 1977, Complex formation resistivity—the forgotton half of the resistivity log: Soc. Prof. Well Log Analysts 18th Ann. Logging Symp., Houston, paper Z.

Sumner, J. S., 1976, Principles of induced polarization for geophysical exploration: Elsevier Science Publ. Co.

Van Voorhis, G. D., Nelson, P. H., and Drake, T. L., 1973, Complex resistivity spectra of porphyry copper mineralization: Geophysics, **38**, 49–60.

Vinegar, H. J., and Waxman, M. H., 1982, Method and apparatus for determining shaliness and oil saturations in earth formations using induced polarization in the frequency domain: U.S. Patent no. 4,359,687, November 16.

——— 1984, Induced polarization in shaly sands: Geophysics, **49**, 1267–1287.

Vinegar, H. J., Waxman, M. H., Best, M. H., and Reddy, I. K., 1985, Induced polarization logging—tool development, borehole departure curves and field test results: Soc. Prof. Well Log Analysts, 26th Ann. Logging Symp., Dallas, paper AAA.

Wait, J. R., 1959, The variable frequency method, *in* Wait, J. R., Ed., Overvoltage research and geophysical applications: Pergamon Press, 29–49.

Wynn, J. C. and Zonge, K. L., 1977, Electromagnetic coupling: Geophys. Prosp., **25**, 29–51.

Zonge, K. L., Sauck, W. A., and Sumner, J. S., 1972, Comparison of time, frequency and phase measurements in induced polarization: Geophys. Prosp., **20**, 626–648.

APPENDIX A

SOLUTION OF THE FORWARD PROBLEM

This appendix solves our dynamic model equations for electrode-type electrical logging devices in the two logging geometries considered in this report. As discussed, these solutions are used to calculate apparent resistivities (R_a) and phase angles (θ_a) for the theoretical tool response.

Infinitely thick noninvaded bed penetrated by a borehole

The model equations solved here were discussed in the text. Recall that the vector potential **A** obeys the inhomogeneous wave equation

$$\nabla^2\mathbf{A} + k^2\mathbf{A} = -\mathbf{J}_s(\mathbf{r}), \tag{A-1}$$

where the source current density $\mathbf{J}_s(\mathbf{r})$ is given by

$$\mathbf{J}_s(\mathbf{r}) = -\frac{I\delta(\rho)[u(z) - u(z-L)]\mathbf{e}_z}{2\pi\rho}, \tag{A-2}$$

where all quantities in equations (A-1) and (A-2) have been defined previously. The vector potential is a vector of the form $\mathbf{A} = (0, 0, A)$ because the source current density is in the z direction. If A_1 denotes the solution of the above equations in the borehole, then A_1 obeys the equation

$$\nabla^2 A_1 + k_1^2 A_1 = \frac{I\delta(\rho)[u(z) - u(z-L)]}{2\pi\rho} \tag{A-3}$$

valid for $\rho \le a$. If A_2 denotes the solution outside of the borehole, then A_2 obeys the equation

$$\nabla^2 A_2 + k_2^2 A_2 = 0, \tag{A-4}$$

for $\rho \geq a$. In equations (A-3) and (A-4), k_ℓ(for $\ell = 1, 2$) denotes the complex propagation constant of the ℓth medium defined by

$$k_\ell = \frac{(1+i)}{\delta_\ell}(1 - i\theta_\ell)^{1/2}, \tag{A-5}$$

where $\delta_\ell = (2/\omega\mu_0\sigma_\ell)^{1/2}$ and $\theta_\ell = \omega\varepsilon'_\ell/\sigma_\ell$ are the classical skin depth and IP parameter, respectively, of the medium. To solve equations (A-3) and (A-4), specify the correct boundary conditions at $\rho = a$. The boundary conditions on the vector potential are obtained from the requirement that the tangential components of **E** and **H** be continuous at $\rho = a$. That is, impose the conditions

$$E_{1z} = E_{2z} \tag{A-6a}$$

and

$$H_{1\phi} = H_{2\phi} \tag{A-6b}$$

at $\rho = a$. From equations (12), (14), and (16),

$$E_{\ell z} = \frac{1}{\sigma_\ell^*}\frac{\partial^2 A_\ell}{\partial z^2} + i\omega\mu_0 A_\ell, \tag{A-7}$$

and

$$H_{\ell\phi} = \frac{\partial A_\ell}{\partial \rho}, \tag{A-8}$$

where $\sigma_\ell^* = \sigma_\ell - i\omega\varepsilon'_\ell$ for $\ell = 1, 2$. If equations (A-7) and (A-8) are combined, then the boundary conditions at $\rho = a$ are equivalent to the conditions

$$\left(\frac{1}{\sigma_1^*}\frac{\partial^2 A_1}{\partial z^2} + i\omega\mu_0 A_1\right)_{\rho=a} = \left(\frac{1}{\sigma_2^*}\frac{\partial^2 A_2}{\partial z^2} + i\omega\mu_0 A_2\right)_{\rho=a}, \tag{A-9}$$

and

$$\left(\frac{\partial A_1}{\partial \rho}\right)_{\rho=a} = \left(\frac{\partial A_2}{\partial \rho}\right)_{\rho=a}. \tag{A-10}$$

Green's functions

To solve equations (A-3) and (A-4) subject to the boundary conditions given in equations (A-9) and (A-10), it is convenient to introduce Green's functions $G_\ell(\rho, z - z')$ for $\ell = 1, 2$. The Green's functions satisfy the equations

$$\nabla^2 G_1 + k_1^2 G_1 = \frac{I\delta(\rho)\delta(z - z')}{2\pi\rho}, \tag{A-11}$$

for $\rho \leq a$ and

$$\nabla^2 G_2 + k_2^2 G_2 = 0 \tag{A-12}$$

for $\rho \geq a$. We seek solutions of equations (A-11) and (A-12) subject to the boundary conditions

$$\left(\frac{1}{\sigma_1^*}\frac{\partial^2 G}{\partial z^2} + i\omega\mu_0 G_1\right)_{\rho=a} = \left(\frac{1}{\sigma_2^*}\frac{\partial^2 G_2}{\partial z^2} + i\omega\mu_0 G_2\right)_{\rho=a}, \tag{A-13}$$

and

$$\left(\frac{\partial G_1}{\partial \rho}\right)_{\rho=a} = \left(\frac{\partial G_2}{\partial \rho}\right)_{\rho=a} \tag{A-14}$$

A solution of equation (A-11) which is regular at $\rho = 0$ can be written in the form (valid for $\rho \leq a$)

$$G_1 = \frac{-Ie^{ik_1 R}}{4\pi R} + \int_0^\infty d\lambda\, B(\lambda) I_0(\gamma_1\rho)\cos\lambda(z - z'), \tag{A-15}$$

where the first term is a solution of the inhomogeneous differential equation and the second term satisfies the homogeneous equation. The function I_0 is a zeroth-order modified Bessel function of the first kind, and $\gamma_1 = \sqrt{\lambda^2 - k_1^2}$ and $R = \sqrt{\rho^2 + (z - z')^2}$. A solution of equation (A-12) which is regular at $\rho = \infty$ can be written in the form (valid for $\rho \geq a$)

$$G_2 = \int_0^\infty d\lambda\, C(\lambda) K_0(\gamma_2\rho)\cos\lambda(z - z'), \tag{A-16}$$

where K_0 is a zeroth-order modified Bessel function of the second kind and $\gamma_2 = \sqrt{\lambda^2 - k_2^2}$. The functions $B(\lambda)$ and $C(\lambda)$ are chosen so that the boundary conditions at $\rho = a$ are satisfied.

The rationale for introducing the Green's functions $G_\ell(\rho, z - z')$ is that the vector potentials $A_\ell(\rho, z)$ can be expressed in terms of the functions G_ℓ by the integral

$$A_\ell(\rho, z) = \int_0^L dz'\, G_\ell(\rho, z - z'), \tag{A-17}$$

valid for $\ell = 1, 2$. This simplifies the problem because the inhomogeneous equation (A-11) satisfied by G_1 is easier to solve than the inhomogeneous equation (A-3) satisfied by A_1. Furthermore, the functions A_ℓ defined in equation (A-17) will automatically satisfy the proper boundary conditions.

The next step in the calculation of the functions A_ℓ is to solve for the functions $B(\lambda)$ and $C(\lambda)$. It is convenient to introduce the mathematical identity

$$\frac{e^{ik_1 R}}{R} \equiv \frac{2}{\pi}\int_0^\infty d\lambda\, K_0(\gamma_1\rho)\cos\gamma(z - z') \tag{A-18}$$

which can be proven using the theory of integral transforms. If equation (A-18) is substituted into equation (A-15) and recall equation (A-16), then after some algebra, the boundary condition in equation (A-13) leads to the equation

$$-\gamma_1^2 I_0(\gamma_1 a)B(\lambda) + \frac{\sigma_1^*}{\sigma_2^*}\gamma_2^2 K_0(\gamma_2 a)C(\lambda) = \frac{-I}{2\pi^2}\gamma_1^2 K_0(\gamma_1 a). \tag{A-19}$$

Similarly, the boundary condition in equation (A-14) leads to the equation

$$\gamma_1 I_1(\gamma_1 a)B(\lambda) + \gamma_2 K_1(\gamma_2 a)C(\lambda) = \frac{-I}{2\pi^2}\gamma_1 K_1(\gamma_1 a), \tag{A-20}$$

where I_1 and K_1 are first-order modified Bessel functions of the first and second kinds, respectively. In arriving at equation (A-20), we have used the well-known relations

$$\frac{dI_0(z)}{dz} = I_1(z), \tag{A-21a}$$

and

$$\frac{dK_0(z)}{dz} = -K_1(z), \tag{A-21b}$$

where z is a complex argument. The functions $B(\lambda)$ and $C(\lambda)$ are solutions of the algebraic equations (A-19) and (A-20). We

are interested in calculating the voltage components (i.e., $V_{MN,I}$ and $V_{MN,Q}$) induced between the M and N electrodes. Therefore, we are interested in the solution of $A_1(\rho, z)$ which involves the function $B(\lambda)$.

To save space we do not give our result for $C(\lambda)$, since we do not explicitly use $A_2(\rho, z)$. On solving the simultaneous equations (A-19) and (A-20) for $B(\lambda)$,

$$B(\lambda) = \frac{\frac{I}{2\pi^2}\left[\gamma_1 K_0(\gamma_1 a)K_1(\gamma_2 a) - \gamma_2 \frac{\sigma_1^*}{\sigma_2^*} K_0(\gamma_2 a)K_1(\gamma_1 a)\right]}{\left[\gamma_1 I_0(\gamma_1 a)K_1(\gamma_2 a) + \frac{\sigma_1^*}{\sigma_2^*}\gamma_2 I_1(\gamma_1 a)K_0(\gamma_2 a)\right]}. \tag{A-22}$$

On combining equations (A-15) and (A-17), we find that $A_1(\rho, z)$ can be written in the form

$$A_1(\rho, z) = \frac{-I}{4\pi}\int_0^L \frac{dz'\, e^{ik_1 R}}{R} + \int_0^\infty \frac{d\lambda}{\lambda} B(\lambda) I_0(\gamma_1 \rho)[\sin \lambda z - \sin \lambda(z - L)], \tag{A-23}$$

with $B(\lambda)$ given by equation (A-22). The complex voltage V_{MN} induced in the cable connecting the M and N measuring electrodes is given by the line integral

$$V_{MN} = \int_{z_M}^{z_N} dz\, E_1(\rho_0, z) \equiv \int_{z_M}^{z_N} dz \left(\frac{1}{\sigma_1^*}\frac{\partial^2 A_1}{\partial z^2} + i\omega\mu_0 A_1\right), \tag{A-24}$$

where the integration is along a line $\rho = \rho_0$ where ρ_0 is the radial coordinate of the measuring cables and $z_M = AM$ and $z_N = AN$ are electrode spacings. The real and imaginary components of V_{MN} are the in-phase ($V_{MN,I}$) and quadrature ($V_{MN,Q}$) induced voltage components, respectively. That is,

$$V_{MN,I} = \text{Re}\,(V_{MN}) = \text{Re}\,[V(\rho_0, z_N) - V(\rho_0, z_M)] \tag{A-25a}$$

$$V_{MN,Q} = \text{Im}\,(V_{MN}) = \text{Im}\,[V(\rho_0, z_N) - V(\rho_0, z_M)] \tag{A-25b}$$

where the complex voltage $V(\rho_0, z)$ is obtained from performing the indefinite integral in equation (A-24). Calculation of $V(\rho_0, z)$ is straightforward, although somewhat tedious. With the aid of equations (A-23) and (A-24),

$$V(\rho_0, z) = \frac{I}{4\pi\sigma_1^*}\left(\frac{e^{ik_1 s_L}}{s_L} - \frac{e^{ik_1 s}}{s}\right) + \frac{I}{\sigma_1^*}\int_0^\infty \frac{d\lambda}{\lambda^2}\gamma_1^2(\lambda)B(\lambda)I_0(\gamma_1\rho_0) \times \left[\cos \lambda z - \cos \lambda(z - L)\right] - \frac{Ik_1^2 z}{2\pi\sigma_1^*} K_0(-ik_1\rho_0) - \frac{ik_1 I}{4\pi\sigma_1^*}\left\{E_2(-ik_1 z) - E_2[-ik_1(L - z)]\right\}, \tag{A-26}$$

where

$$s_L = \sqrt{\rho_0^2 + (L - z)^2},$$

and

$$s = \sqrt{\rho_0^2 + z^2},$$

and where E_2 is the exponential integral defined for complex argument z^* by

$$E_2(z^*) = \int_1^\infty \frac{dt\, e^{-z^* t}}{t^2}, \tag{A-27}$$

for Re $z^* > 0$. The third and fourth terms in equation (A-26) represent dynamic contributions to $V(\rho_0, z)$ arising from EM effects. Note that these terms vanish in the limit of zero frequency and therefore are not present in the static potential theory of electrode type resistivity devices (Dakhnov, 1959). On taking the limit $\omega \to 0$ and setting $\theta_\ell = 0$ (for $\ell = 1, 2$), equation (A-26) reduces (as expected) to the result the static potential theory would produce.

The dependence of $V(\rho_0, z)$ on the formation IP parameter θ_2 is contained in the second term [i.e., in the function $B(\lambda)$ of equation (A-26)]. The term contains the IP effect of the formation. The EM coupling effects on the apparent phase angles θ_a are dominated by the K_0 term in equation (A-26). The terms in equation (A-26), except for the integral, are identical to the terms for a homogeneous medium having the electrical properties of the drilling mud [e.g., see equation (B-14)]. The EM contributions to θ_a are calculated as described in the text. That is, the EM contribution is a function of frequency f and is defined by

$$\Delta\theta = \theta_a(f) - \theta_a(f_0), \tag{A-28}$$

where $\Delta\theta$ is the EM effect at frequency f and f_0 is a low frequency for which EM effects are negligible. In our numerical computations of $\Delta\theta$, we used a value $f_0 = 2^{-6}$ (0.015 6) Hz. As noted, we verified numerically that the EM effects are independent of the formation IP parameters for the range of interest in shaly sands (i.e., less than 30 mradians).

Infinitely thick invaded bed penetrated by a borehole

Here we solve our model equations for a simple three-region model in which the annular region $a \le \rho \le b$ is invaded by borehole fluids. Here b is the radius of the invaded zone, and region $\rho > b$ represents the uninvaded formation. The calculation of $V(\rho_0, z)$ for this situation follows the same pattern as the calculation for an infinitely thick noninvaded bed; therefore, some of the details are omitted.

The vector potentials A_ℓ (for $\ell = 1, 2, 3$) in the three regions of interest obey the equations

$$\nabla^2 A_1 + k_1^2 A_1 = \frac{I\delta(\rho)}{2\pi\rho}\left[u(z) - u(z - L)\right], \tag{A-29}$$

for $\rho \le a$,

$$\nabla^2 A_2 + k_2^2 A_2 = 0, \tag{A-30}$$

for $a \le \rho \le b$, and

$$\nabla^2 A_3 + k_3^2 A_3 = 0, \tag{A-31}$$

for $\rho \ge b$. The boundary conditions on the functions A_ℓ are obtained from equations (A-7) and (A-8), together with the conditions on the EM field vectors, i.e.,

$$E_{1z} = E_{2z}. \qquad \text{at } \rho = a, \tag{A-32a}$$

$$H_{1\phi} = H_{2\phi}, \quad \text{at } \rho = a, \tag{A-32b}$$

$$E_{2z} = E_{3z}, \quad \text{at } \rho = b, \tag{A-32c}$$

and

$$H_{2\phi} = H_{3\phi}, \quad \text{at } \rho = b. \tag{A-32d}$$

The next step in the solution of the equations (A-29)–(A-31) we introduce the Green's functions $G_\ell(\rho, z - z')$ defined by the equations,

$$\nabla^2 G_1 + k_1^2 G_1 = \frac{I\delta(\rho)\delta(z - z')}{2\pi\rho}, \tag{A-33}$$

for $0 \le \rho \le a$,

$$\nabla^2 G_2 + k_2^2 G_2 = 0, \tag{A-34}$$

for $a \le \rho \le b$, and

$$\nabla^2 G_3 + k_3^2 G_3 = 0, \tag{A-35}$$

for $\rho \ge b$. The solutions of equations (A-33)–(A-35) can be written in the form

$$G_1 = \frac{-Ie^{ik_1 R}}{4\pi R} + \int_0^\infty d\lambda\, B(\lambda) I_0(\gamma_1 \rho) \cos \lambda(z - z'), \tag{A-36}$$

for $0 \le \rho \le a$,

$$G_2 = \int_0^\infty d\lambda \left[C(\lambda) K_0(\gamma_2 \rho) + D(\lambda) I_0(\gamma_2 \rho) \right] \cos \lambda(z - z'), \tag{A-37}$$

for $a \le \rho \le b$, and

$$G_3 = \int_0^\infty d\lambda\, E(\lambda) K_0(\gamma_3 \rho) \cos \lambda(z - z'), \tag{A-38}$$

for $\rho \ge b$. The functions $B(\lambda)$, $C(\lambda)$, $D(\lambda)$, and $E(\lambda)$ are determined from the boundary conditions imposed on the functions G_ℓ at $\rho = a$ and $\rho = b$. These boundary conditions are identical to those in equations (A-13) and (A-14). Imposing the conditions on equations (A-36)–(A-38) leads to four algebraic equations for the unknown functions:

$$\gamma_1^2 I_0(\gamma_1 a) B - \frac{\sigma_1^*}{\sigma_2^*} \gamma_2^2 \left[K_0(\gamma_2 a) C + I_0(\gamma_2 a) D \right] = \frac{I\gamma_1^2}{2\pi^2} K_0(\gamma_1 a), \tag{A-39a}$$

$$\gamma_1 I_1(\gamma_1 a) B + \gamma_2 \left[K_1(\gamma_2 a) C - I_1(\gamma_2 a) D \right] = \frac{-I}{2\pi^2} \gamma_1 K_1(\gamma_1 a), \tag{A-39b}$$

$$\gamma_2^2 \left[K_0(\gamma_2 b) C + I_0(\gamma_2 b) D \right] - \frac{\sigma_2^*}{\sigma_3^*} \gamma_3^2 K_0(\gamma_3 b) E = 0, \tag{A-39c}$$

and

$$\gamma_2 \left[K_1(\gamma_2 b) C - I_1(\gamma_2 b) D \right] - \gamma_3 K_1(\gamma_3 b) E = 0. \tag{A-39d}$$

As discussed, our solution for $V(\rho_0, z)$ only involves the unknown function $B(\lambda)$. On solving the above equation for $B(\lambda)$,

$$B(\lambda) = \frac{\dfrac{I}{2\pi^2} \left[K_0(\gamma_1 a) H_1(\lambda) - \dfrac{\gamma_2}{\gamma_1} \dfrac{\sigma_1^*}{\sigma_2^*} K_1(\gamma_1 a) H_2(\lambda) \right]}{I_0(\gamma_1 a) H_1(\lambda) - \dfrac{\gamma_2}{\gamma_1} \dfrac{\sigma_1^*}{\sigma_2^*} I_1(\gamma_1 a) H_2(\lambda)}, \tag{A-40}$$

where

$$H_1(\lambda) = K_1(\gamma_2 a) F_1(\lambda) + I_1(\gamma_2 a) F_2(\lambda), \tag{A-41a}$$

$$H_2(\lambda) = K_0(\gamma_2 a) F_1(\lambda) - I_0(\gamma_2 a) F_2(\lambda), \tag{A-41b}$$

with

$$F_1(\lambda) = I_0(\gamma_3 b) K_1(\gamma_3 b) - \frac{\gamma_3}{\gamma_2} \frac{\sigma_2^*}{\sigma_3^*} I_1(\gamma_3 b) K_0(\gamma_3 b), \tag{A-41c}$$

and

$$F_2(\lambda) = 1 - \frac{\gamma_3 \sigma_2^*}{\gamma_2 \sigma_3^*} K_1(\gamma_3 b) K_0(\gamma_3 b). \tag{A-41d}$$

Substituting $B(\lambda)$ into equation (A-26) yields the complex voltage $V(\rho_0, z)$ appropriate to the invasion model discussed here.

B electrode in the mud pit

Here we modify the results of the preceding two subsections to account for the frequent situation where the B electrode is placed in the mud pit. For practical purposes, we are interested in the limit $L \to \infty$ in the results for $V(\rho_0, z)$. From equations (A-15) and (A-17),

$$A_1(\rho, z) = \frac{-I}{4\pi} \int_0^\infty \frac{dz'\, e^{ik_1 R}}{R} + \int_0^\infty dz' \int_0^\infty d\lambda\, B(\lambda) I_0(\gamma_1 \rho) \cos \lambda(z - z'), \tag{A-42}$$

for $L \to \infty$. In Appendix B it is shown that the first term in the above equation can be written in the form

$$\int_0^\infty \frac{dz'\, e^{ik_1 R}}{R} = 2K_0(-ik_1 \rho_0) - E_1(-ik_1 z), \tag{A-43}$$

for $\rho_0 \ll z$, where E_1 is an exponential integral of complex argument defined by equation (B-6). Consider the second term, denoted for convenience by T_2. Interchanging the order of integration results in the equation

$$T_2 = \int_0^\infty d\lambda\, B(\lambda) I_0(\gamma_1 \rho) \int_0^\infty dz' \cos \lambda(z - z'). \tag{A-44}$$

The integral over the variable z' is elementary and leads to the result

$$\int_0^\infty dz' \cos \lambda(z - z') = \frac{\sin \lambda z}{\lambda} + \pi\delta(\lambda), \tag{A-45}$$

where $\delta(\lambda)$ is the Dirac delta function. Combining the results of equations (A-44) and (A-45) yields

$$A_1(\rho_0, z) = \frac{-I}{2\pi} K_0(-ik_1 \rho_0) + \frac{I}{4\pi} E_1(-ik_1 z) + \int_0^\infty \frac{d\lambda}{\lambda} B(\lambda) I(\gamma_1 \rho_0) \sin \lambda z + \frac{\pi B(0)}{2} I_0(-ik_1 \rho_0), \tag{A-46}$$

where $B(0)$ is $B(\lambda)$ evaluated at $\lambda = 0$. Recall that $V(\rho_0, z)$ is defined by the indefinite integral

$$V(\rho_0, z) = \int^z dz'\, E_{1z}(\rho_0, z') \equiv \frac{1}{\sigma_1^*}\frac{\partial A_1}{\partial z} + i\omega\mu_0 \int^z dz'\, A_1(\rho_0, z'), \quad \text{(A-47)}$$

by using equation (A-24). On substituting equation (A-46) into equation (A-47), after some algebra,

$$V(\rho_0, z) = \frac{-I}{4\pi\sigma_1^*}\frac{e^{ik_1 z}}{z} + \frac{1}{\sigma_1^*}\int_0^\infty \frac{d\lambda\, \gamma_1^2}{\lambda^2} B(\lambda) I_0(\gamma_1\rho_0)\cos\lambda z - \frac{Ik_1^2 z}{2\pi\sigma_1^*} K_0(-ik_1\rho_0) - \frac{ik_1 I}{4\pi\sigma_1^*} E_2(-ik_1 z) + \frac{\pi k_1^2 z}{2\sigma_1^*} B(0) I_0\left[\gamma_1(0)\rho_0\right]. \quad \text{(A-48)}$$

APPENDIX B

SOLUTION OF THE DYNAMIC MODEL IN AN INFINITE HOMOGENEOUS MEDIUM

Derivation of complex voltage

Appendix A focused on the solution of the boundary-value problems associated with solutions of the dynamic model equations in the two logging geometries considered. The origin and derivation of the dynamic coupling contributions to the measured voltages were perhaps somewhat obscured by the details associated with the boundary-value problems. To gain insight and avoid these complications, we solve the dynamic model equations in an infinite homogeneous medium and compare the results with previous work (Wait, 1959).

The z-component of the vector potential obeys the equation

$$\nabla^2 A + k^2 A = -J_s(\mathbf{r}), \quad \text{(B-1)}$$

where the source current density is given in equation (A-2). The solution of equation (B-1) in an infinite homogeneous medium has the form

$$A(\mathbf{r}) = \int \frac{d^3\mathbf{r}'}{4\pi}\frac{\exp(ik|\mathbf{r}-\mathbf{r}'|)}{|\mathbf{r}-\mathbf{r}'|} J_s(\mathbf{r}'), \quad \text{(B-2)}$$

where in cylindrical coordinates (ρ, ϕ, z),

$$|\mathbf{r}-\mathbf{r}'| = \sqrt{\rho^2 - \rho'^2 - 2\rho\rho'\cos(\phi-\phi') + (z-z')^2}.$$

Combining equations (B-1) and (B-2) and using equation (A-2) results in

$$A(\rho, z) = \frac{-I}{4\pi}\int_0^L \frac{dz'\exp\left[ik\sqrt{\rho^2+(z-z')^2}\right]}{\sqrt{\rho^2+(z-z')^2}}. \quad \text{(B-3)}$$

From the change of variables $\lambda = (z'-z)/\delta$, the above integral can be written in the form

$$A(\rho, z) = \frac{-I}{4\pi}\left[2\int_0^\infty \frac{d\lambda\, e^{(1-i)u}}{u} - \int_{z/\delta}^\infty \frac{d\lambda\, e^{-(1-i)u}}{u} - \int_{(L-z)/\delta}^\infty \frac{d\lambda\, e^{-(1-i)u}}{u}\right], \quad \text{(B-4)}$$

where $u = \sqrt{\lambda^2 + (\rho/\delta)^2}$. In equation (B-4) we have assumed $k \equiv (1+i)/\delta$, where $\delta = (2/\omega\mu_0\sigma)^{1/2}$ is the classical skin depth. This implies that the IP parameter of the medium is zero, and is valid since the coupling effects are dominated by the conductivity of the medium for systems of interest here. The first integral in equation (B-4) can be expressed in terms of a zeroth-order modified Bessel function. The second and third integrals can be simplified in cases for which $z \gg \rho$ and $L - z \gg \rho$. In these cases u can be replaced by λ in the integrals, and $\bar{\lambda} = \lambda(\delta/z)$ and $\bar{\lambda} = \lambda\delta/(L-z)$ in the second and third integrals, respectively. This results in the equation

$$A(\rho, z) = \frac{-I}{4\pi}\left\{2K_0(-ik\rho) - E_1(-ikz) - E_1[-ik(L-z)]\right\}, \quad \text{(B-5)}$$

where the exponential integral functions E_1 are defined by

$$E_n(z^*) = \int_1^\infty \frac{dt\, e^{-z^* t}}{t^n}, \quad \text{(B-6)}$$

valid for $n = (0, 1, 2, 3 \ldots)$ with z^* a complex argument such that $\mathrm{Re}\, z^* > 0$.

To calculate the induced voltage V_{MN} between the measuring electrodes the line integral must be computed:

$$V_{MN} = \int_{z_M}^{z_N} d\ell \cdot \mathbf{E}(\rho_0, z) \equiv \int_{z_M}^{z_N} d\ell \cdot (-\nabla\Phi + i\omega\mu_0 \mathbf{A}), \quad \text{(B-7)}$$

where $d\ell = \mathbf{e}_z\, dz$ and $\rho = \rho_0$. On performing the integral for the term involving the scalar potential,

$$V_{MN} = \Phi_M - \Phi_N + i\omega\mu_0 \int_{z_M}^{z_N} dz\, A(\rho_0, z). \quad \text{(B-8)}$$

The scalar potential can be obtained from the gauge condition

$$\Phi = -\frac{1}{\sigma}\nabla\cdot\mathbf{A}. \quad \text{(B-9)}$$

Using the above equation and equation (B-3), it is easy to demonstrate that

$$\Phi_M \equiv \Phi(\rho_0, z_M) = \frac{I}{4\pi\sigma}\left[\frac{\exp(ik\sqrt{\rho_0^2+z_M^2})}{\sqrt{\rho_0^2+z_M^2}}\right.$$

$$-\frac{\exp\left(ik\sqrt{\rho_0^2+(L-z_M)^2}\right)}{\sqrt{\rho_0^2+(L-z_M)^2}}\Bigg], \qquad \text{(B-10)}$$

and similarly for Φ_N. Consider the integral in equation (B-8), i.e.,

$$\int_{z_M}^{z_N} dz\, A(\rho_0, z)$$

$$= \frac{-I}{4\pi}\int_{z_M}^{z_N} dz\left[2K_0(-ik\rho_0) - E_1(-ikz) - E_1\left[-ik(L-z)\right]\right]. \qquad \text{(B-11)}$$

To perform the integral in equation (B-11), use a recurrence relation obeyed by the exponential integral functions of complex argument z^* (Erdelyi, 1954):

$$\frac{dE_n(z^*)}{dz^*} = -E_{n-1}(z^*), \qquad \text{(B-12)}$$

valid for $n = (1, 2, \ldots)$. Thus the exponential integral functions in the integrand of equation (B-11) can be written in the form

$$E_1(-ikz) = (ik)^{-1}\frac{dE_2}{dz}(-ikz),$$

and $\qquad \text{(B-13a)}$

$$E_1[-ik(L-z)] = -(ik)^{-1}\frac{dE_2}{dz}[-ik(L-z)],$$

On substitution of the values from equation (B-13a) into equation (B-11), the integrals are elementary and

$$V_{MN} = \Phi_M - \Phi_N - \frac{I}{4\pi\sigma}\Bigg(2k^2(z_N - z_M)K_0(-ik\rho_0) + ik\Big\{E_2(-ikz_N) - E_2(-ikz_M) - E_2[-ik(L-z_N)] + E_2[-ik(L-z_M)]\Big\}\Bigg), \qquad \text{(B-14)}$$

from equation (B-8). The scalar potential terms Φ_M and Φ_N are defined by equation (B-10). The scalar potential terms reduce in the limit of zero frequency to the same result (for an infinite homogeneous medium) as in the conventional static potential theory of resistivity logging. The terms in parentheses in equation (B-14) represent the EM coupling between the current and measuring electrode cables; these terms vanish in the limit of zero frequency, and therefore they represent "primary" dynamic contributions to the measured voltages. These contributions arise from the time derivative of the vector potential and therefore have no opportunity to appear in a static theory. The quadrature voltages (i.e., $V_{MN,Q} = \text{Im } V_{MN}$), and therefore the apparent phase angles (θ_a), contain EM coupling effects which can mimic the IP response of earth formations. As noted previously, these contributions must be properly accounted for in quantitative IP logging of shaly sand petroleum reservoirs to get an acceptable degree of accuracy. Wait (1959) gives expressions [Wait's equations (40)–(42), p. 40] for the transfer impedance $z = V/I$, between parallel current and voltage cables in a homogeneous medium. It can be shown that V_{MN}/I in equation (B-14) is identical to the result from Wait's expressions by making the following substitutions: $\rho = \rho_0$, $C_1 = 0$, $C_2 = L$, $P_1 = z_M$, $P_2 = z_N$, and $\gamma = -ik$ and then performing the indicated integrations.

EM contribution to apparent resistivity

From equation (B-14) expressions for the apparent resistivity of the medium, including EM contributions can be obtained. We derive here a simple expression valid in the limit $z_N \ll \delta$, $z_M \ll \delta$, and $L \to \infty$ (e.g., B electrode in the mud pit). The apparent resistivity is given by

$$R_a(\omega) = \frac{4\pi}{I}\left(\frac{1}{z_M} - \frac{1}{z_N}\right)^{-1} V_{MN,I} \qquad \text{(B-15)}$$

where the frequency dependence of $R_a(\omega)$ is explicitly indicated. The small-argument expansions of the functions K_0 and E_2 are needed in equation (B-14). The first few terms of these expansions for the complex argument z^* are (Abramowitz and Stegun, 1964),

$$K_0(z^*) = -\left(\ln\frac{z^*}{2} + \gamma\right)\left(1 + \frac{z^{*2}}{4} + \cdots\right) + \frac{z^{*2}}{4} + \cdots, \qquad \text{(B-16)}$$

and

$$E_2(z^*) = z^*(\ln z^* + \gamma - 1) + 1 - \frac{z^{*2}}{2} + \cdots, \qquad \text{(B-17)}$$

where $\gamma = 0.577\,215\,664\,9$ is Euler's constant. The expansions in equations (B-16) and (B-17), together with equations (B-14) and (B-15), yield, after some algebra,

$$R_a(\omega) \simeq R_a(0)\left(1 + \frac{\pi}{2}\frac{z_M z_N}{\delta^2} + \cdots\right), \qquad \text{(B-18)}$$

where $R_a(0)$ is the apparent resistivity at zero frequency. Note that here $R_a(0) = R = \sigma^{-1}$, the true resistivity of the medium, because we are considering an infinite homogeneous medium. The "skin effect" (i.e., EM effect) contribution is given by the second term in parentheses in the equation. Note that this contribution is directly proportional to the frequency. For electrode-type resistivity tools with long electrode spacings, the EM contributions can become very large. These effects can be minimized by operating the tools at very low frequencies. The ULSEL tools (Runge et al., 1969) are operated at 0.05 Hz to minimize the EM effects. Moran and Gianzero (1979) have given a formula similar to equation (B-18); however, our result differs from theirs in the sign of the skin-effect correction. This discrepancy can be traced to a sign error in the exponential functions in their equation (38).

APPENDIX C

DERIVATION OF A NONLINEAR RELATIONSHIP BETWEEN IP PHASE ANGLE AND PERCENT FREQUENCY EFFECT

Nonlinear relationship

In this appendix we derive an approximate relationship between the two most commonly used IP parameters, phase angle and percent frequency effect (PFE). Phase angle in IP is defined as the difference in phase between the input current and the measured voltage response assuming sinusoidal waveforms for both.

In terms of a complex voltage $V(\omega)$, the phase angle at frequency ω is given by the arctangent of the ratio of the imaginary component of the voltage to the real component. That is, the phase angle $\theta(\omega)$ at frequency ω is

$$\theta(\omega) = \tan^{-1} \frac{\text{Im } V(\omega)}{\text{Re } V(\omega)}. \qquad \text{(C-1)}$$

PFE is a parameter computed from measurement of the voltage amplitude (i.e., peak voltage) at two different frequencies, a low frequency (ω_1) and a high frequency (ω_2). The definition of PFE is

$$\text{PFE} \equiv 100\ \text{FE} = 100 \frac{|V(\omega_2)| - |V(\omega_1)|}{|V(\omega_1)|}, \qquad \text{(C-2)}$$

where $|V(\omega_2)|$ and $|V(\omega_1)|$ are the high and low frequencies measured voltage amplitudes, respectively. In equation (C-2) we introduced the frequency effect (FE), which is simply the PFE divided by 100. In definition (C-2) of PFE, it is understood that the input current amplitude is independent of frequency. Therefore, in equation (C-2) the voltage amplitudes can be replaced with the corresponding apparent resistivities without altering the definition of PFE.

In the derivation of a relation between PFE and phase angle, the PFE is calculated using frequencies a decade apart, that is, $\omega_2 = 10\omega_1$. The starting point is an approximate relationship given by Zonge et al. (1972),

$$\theta(\omega) \simeq \frac{\pi}{2} \frac{d \ln |V(\omega)|}{d \ln \omega}. \qquad \text{(C-3)}$$

A derivation of the above relation has been given by Balabanian and Bickart (1969). Laboratory experiments on IP in rocks have shown that $\theta(\omega)$ has a weak dependence on frequency. Indeed, the data of Zonge et al. (1972) suggest that over a decade interval of frequency the phase angle varies approximately linearly with the logarithm of the frequency. Therefore, we assume in the frequency interval $\omega_1 \le \omega \le 10\omega_1$ that

$$\theta(\omega) \simeq \theta(\omega_1) + [\theta(\omega_2) - \theta(\omega_1)] \frac{\ln \dfrac{\omega}{\omega_1}}{\ln \dfrac{\omega_2}{\omega_1}}. \qquad \text{(C-4)}$$

On substitution of expression (C-4) into expression (C-3) and integrating from ω_1 to ω_2, after some algebra,

$$\ln \frac{|V(\omega_2)|}{|V(\omega_1)|} = \frac{2}{\pi} \frac{\theta(\omega_1) + \theta(\omega_2)}{2} \ln \frac{\omega_2}{\omega_1}. \qquad \text{(C-5)}$$

It follows from expression (C-4) that at $\omega = \sqrt{\omega_1\omega_2}$

$$\theta(\sqrt{\omega_1\omega_2}) = \frac{\theta(\omega_1) + \theta(\omega_2)}{2}. \qquad \text{(C-6)}$$

On combining equations (C-5) and (C-6) and recalling equation (C-2), the desired relation is

$$\text{PFE} \equiv 100\ \text{FE} = 100\left[\exp\left(\frac{2\theta}{\pi} \ln \frac{\omega_2}{\omega_1}\right) - 1\right], \qquad \text{(C-7)}$$

where the phase angle is evaluated at the geometric mean ($\omega = \sqrt{\omega_1\omega_2}$) of the two frequencies. Note that PFE is not in general linearly related to phase angle. A linear relation is valid only in the regime of small phase angles or, more precisely, when $2\theta/\pi \ln \omega_2/\omega_1 \ll 1$. In this limit the exponential in equation (C-7) can be expanded to obtain the relationship

$$\text{PFE} \equiv 100\ \text{FE} \simeq 146.6\ \theta \qquad \text{(radians)}, \qquad \text{(C-8a)}$$

or

$$\text{PFE} = 100\ \text{FE} \simeq 0.146\ 6\ \theta \qquad \text{(milliradians)}, \qquad \text{(C-8b)}$$

valid for $2\theta/\pi \ln \omega_2/\omega_1 \ll 1$. The small-phase angle approximation is applicable to the experiments of Vinegar and Waxman (1984) on a suite of 20 shaly sand core samples. The proportionality constant in equation (C-8b) is in good agreement with the experimental value of 0.144 reported by Vinegar and Waxman (1984).

Zonge et al. (1972) relationship

Zonge et al. (1972) have also derived a theoretical relationship between PFE and phase angle using equation (C-3) as their starting point. The relationship they obtained is significantly different from ours because of different approximations and assumptions. Zonge et al. (1972) replace differentials with differences in equation (C-3) and establish the approximate relation

$$\text{PFE} \simeq \frac{200\ \Delta\omega}{\pi\omega}\ \theta, \qquad \text{(C-9)}$$

where $\omega = \sqrt{\omega_1\omega_2} = \omega_1\sqrt{10}$ and $\Delta\omega = \omega_2 - \omega_1$, so that

$$\text{PFE} \simeq 181.1\ \theta \qquad \text{(radians)}, \qquad \text{(C-10a)}$$

or

$$\text{PFE} \simeq 0.181\ 1\ \theta \qquad \text{(milliradians)}. \qquad \text{(C-10b)}$$

It is clear that this result differs considerably from ours and also from the experimental relationship reported by Vinegar and Waxman (1984). Furthermore, Zonge et al. (1972) have reported experimental values of FE and phase angles on a suite of rocks. These experiments were performed on rocks whose IP phase angles spanned a large range, from a few milliradians to several hundred milliradians. In Table 2 the nonlinear (NL) relationship derived here and the Zonge et al. (1972) relationship are compared with these data. It is evident that the theoretical relationship derived here [equations (C-7) and (C-8)] is in better agreement with these data than is the linear relationship derived by Zonge et al. (1972).

APPENDIX D

A METHOD FOR SOLVING THE INVERSE INVASION PROBLEM FOR AN IP LOGGING DEVICE

The determination of unknown formation parameters from logging data involves the solution of an "inverse problem." In this appendix we describe a method for solving the inverse problem for a simple model of a formation invaded by mud filtrate. The method is general and can be applied easily to more complex models of invaded formations.

The model consists of a borehole of known radius $r = a$ containing drilling mud of known resistivity R_m and IP parameter $\theta_m = 0$. The annular region $a \le r \le r_{x0}$ is assumed to be invaded with mud filtrate and to have electrical parameters R_{x0} and θ_{x0}. The uninvaded formation ($r > r_{x0}$) has electrical parameters θ_t and R_t. For this simple model of the invasion, the unknown parameters to be determined are r_{x0}, R_{x0}, R_t, θ_{x0}, and θ_t.

Determination of these parameters requires (1) at least five independent measurements of the response of an IP tool, (2) a computer program that can simulate the response of an IP tool if the parameters of the model described above were known (e.g., a solution of the forward problem discussed in appendix A), and (3) a systematic method for combining the measured logging data with the computer simulation program to obtain the unknown parameters of interest. For an IP tool, we consider a normal type of electrical logging tool operating at a single frequency (in the frequency range of 32 Hz or below) which consists of a source electrode A, a sink electrode B, and three sets of measuring electrode pairs M and N. The tool should have the capability to measure both the in-phase and out-of-phase (with respect to the source current) potential differences between the three electrode pairs. Let $V^{(i)}_{M,I}$ and $V^{(i)}_{M,Q}$ denote the in-phase and out-of-phase measured potential differences for the ith electrode pair ($i = 1, 2, 3$). The negligible dependence of the in-phase voltage (potential difference) in shaly sands on the IP parameters θ_{x0} and θ_t leads to a simplification of the inverse problem.

The inverse resistivity problem can be solved by ignoring the dependence of the in-phase voltage on the IP parameters. The resistivities and invaded zone radius thus determined from this inverse problem can be used to solve for θ_{x0} and θ_t.

Let $V^{(i)}(R_1, R_2, b)$ denote the in-phase potential difference calculated using the computer program which simulates the response of the IP tool where R_1, R_2, and b correspond to the invaded-zone resistivity, the formation resistivity, and the invaded-zone radius, respectively. We choose values of R_1, R_2, and b such that

$$V^{(i)}(R_1, R_2, b) - V^{(i)}_{M,I} \equiv 0, \tag{D-1}$$

for $i = 1, 2, 3$. Application of the Newton-Raphson method to equation (D-1) leads to a set of algebraic recursion relations

$$\Delta R_1^{n+1} \frac{\partial V^{(i)}_n}{\partial R_1^n} + \Delta R_2^{n+1} \frac{\partial V^{(i)}_n}{\partial R_2^n} + \Delta b^{n+1} \frac{\partial V^{(i)}_n}{\partial b^n} = -V^{(i)}_n + V^{(i)}_{M,I}, \tag{D-2}$$

for $i = 1, 2, 3$ where $V^{(i)}_n = V^{(i)}(R_1^n, R_2^n, b^n)$, $\Delta R_1^{n+1} = R_1^{n+1} - R_1^n$, etc. As noted earlier, on convergence of the above equations after M iterations, the desired model parameters, i.e., $R_{x0} = R_1^M$, $R_t = R_2^M$ and $r_{x0} = b^M$, are obtained. Note that the terms in equation (D-2) are identical to equations (29) since the apparent resistivities are proportional to the in-phase voltages.

The next step is to determine the IP parameters θ_{x0} and θ_t. Let

$$\bar{\theta}^{(i)}_M = \tan^{-1} \frac{V^{(i)}_{M,Q}}{V^{(i)}_{M,I}} \tag{D-3}$$

denote the measured phase angle (in radians) for the ith electrode pair from which EM coupling terms have been subtracted. Recall the approximate relation in equation (C-3) which, for constant current amplitude, gives the relations

$$\theta_{x0} \cong \frac{\pi}{2} \frac{d \ln R_{x0}}{d \ln \omega}, \tag{D-4}$$

and

$$\theta_t \cong \frac{\pi}{2} \frac{d \ln R_t}{d \ln \omega}. \tag{D-5}$$

Furthermore, if $\bar{\theta}^{(i)}$ denotes the theoretically computed phase angle for the ith electrode pair, then

$$\bar{\theta}^{(i)} \cong \frac{\pi}{2} \frac{d \ln V^{(i)}(R_{x0}, R_t, r_{x0})}{d \ln \omega}, \tag{D-6}$$

or on taking the indicated derivatives,

$$\bar{\theta}^{(i)} \cong \frac{\pi}{2} \frac{1}{V^{(i)}} \left[R_{x0} \frac{\partial V^{(i)}}{\partial R_{x0}} \frac{d \ln R_{x0}}{d \ln \omega} + R_t \frac{\partial V^{(i)}}{\partial R_t} \frac{d \ln R_t}{d \ln \omega} \right]. \tag{D-7}$$

On substitution of equations (D-4) and (D-5) into the equation (D-7),

$$\bar{\theta}^{(i)} \cong \frac{R_{x0}}{V^{(i)}} \frac{\partial V^{(i)}}{\partial R_{x0}} \theta_{x0} + \frac{R_t}{V^{(i)}} \frac{\partial V^{(i)}}{\partial R_t} \theta_t, \tag{D-8}$$

or on replacing $\bar{\theta}^{(i)}$ by $\bar{\theta}^{(i)}_M$,

$$\bar{\theta}^{(i)}_M \cong \frac{R_{x0}}{V^{(i)}} \frac{\partial V^{(i)}}{\partial R_{x0}} \theta_{x0} + \frac{R_t}{V^{(i)}} \frac{\partial V^{(i)}}{\partial R_t} \theta_t, \tag{D-9}$$

for $i = 1, 2, 3$. The above equation is identical to equation (27) since the apparent resistivities are proportional to the in-phase voltages. Note that any two of the three equations (D-9) should give the unknown values θ_{x0} and θ_t. Any inconsistencies between solutions resulting from choosing different pairs of equations indicates that either the theoretical model is inadequate or the measured data are in error.